NASA Technical Paper 1884

June 1982

Flow Visualization Study of the Horseshoe Vortex in a Turbine Stator Cascade

Raymond E. Gaugler
and Louis M. Russell

NASA

NASA
Technical
Paper
1884

1982

Flow Visualization Study of the Horseshoe Vortex in a Turbine Stator Cascade

Raymond E. Gaugler
and Louis M. Russell

Lewis Research Center
Cleveland, Ohio

NASA
National Aeronautics
and Space Administration

**Scientific and Technical
Information Branch**

SUMMARY

Flow visualization techniques were used to show the behavior of the horseshoe vortex in a large-scale turbine stator cascade. Oil drops on the end-wall surface flowed in response to local shear stresses, indicating the limiting flow streamlines at the surface. Smoke injected into the flow and photographed showed time-averaged flow behavior. Neutrally buoyant helium-filled soap bubbles followed the flow and showed up on photographs as streaks, indicating the paths followed by individual fluid particles. Preliminary attempts to control the vortex were made by injecting air through control jets drilled in the end wall near the vane leading edge. Seventeen different hole locations were tested, one at a time, and the effect of the control jets on the path followed by smoke in the boundary layer was recorded photographically. A motion picture supplement is available.

INTRODUCTION

The heat transfer to the components of a gas turbine is influenced by the various flow mechanisms encountered, as described in the survey paper by Graham (ref. 1). One of the mechanisms, secondary flow, has been shown to have a very pronounced effect, especially on the end-wall surfaces near the intersections with the vanes. Blair (ref. 2) and Graziani et al. (ref. 3) measured the heat transfer from the end wall in a large-scale, two-dimensional turbine rotor cascade and presented Stanton number contour plots. They concluded that the secondary flows greatly influenced the heat transfer on the cascade end wall and on the vane suction surface. They observed especially steep gradients in heat transfer along the end wall near the vane leading edge. As described by Langston et al. (ref. 4) and shown schematically in figure 1, it is in this region that the incoming end-wall boundary layer rolls up into a horseshoe vortex, which then wraps around the leading edge. One leg of this vortex stays close to the suction-side corner as it is swept downstream, while the pressure-side leg is driven across the passage by the pressure difference, as it moves downstream, and becomes part of the passage vortex. Graziani et al. (ref. 3) showed the extent of the influence of this vortex system on their heat transfer results by presenting ink traces of streamlines on the end wall of their cascade.

Aerodynamic investigations of secondary flow patterns have been the object of flow visualization studies for some time. Using smoke, Herzig et al. (ref. 5) observed the rollup of the end-wall boundary layer into a passage vortex, but they did not observe the vortex near the leading edge. They showed very clearly that the deflection of the boundary layer flow from pressure side to suction side varied strongly with distance from the end wall, with the fluid nearer the wall being affected the most. Langston, et al. (ref. 4) made detailed aerodynamic measurements in a large-scale turbine rotor cascade, including end-wall flow visualization and smoke addition to the boundary layer. They observed the streamlines on the end wall associated with the leading-edge horseshoe vortex and noted that all of the smoke introduced into the end-wall inlet boundary layer ended up in the passage vortex. Marchal and Sieverding (ref. 6) used smoke and a laser light sheet to visualize a cross section normal to the flow near the leading edge for both a turbine rotor cascade and a turbine stator cascade. Using this technique they obtained a view of the flow pattern in a plane at an instant in time, but they did not show the spatial development of the vortex.

To provide guidance to the flow analyst, additional insight into the structure of the horseshoe vortex is needed. Thus it was decided to conduct an experimental flow visualization study of the end-wall - leading-edge region to show more detail of the rollup of the turbulent boundary layer into a horseshoe vortex and its relation to the flow traces observed on passage end walls. In addition, a preliminary study was conducted to visualize the local effects on the leading-edge vortex of injecting high-velocity air from holes in the end wall into the boundary layer in the region where the horseshoe vortex originates. This effort was prompted by the encouraging secondary flow control results reported by Goldman and McLallin (ref. 7) in tests of end-wall film cooling.

In the present study a large-scale, two-dimensional turbine stator cascade was used, and the horseshoe vortex was visualized by using two different methods: (1) by injecting a fine stream of smoke into the end-wall boundary layer, which delineates the gross fluid motions in a time-averaged sense, and (2) by injecting neutrally buoyant, helium-filled bubbles into the boundary layer upstream of the cascade and recording the bubble paths as streaks on photographic film. Since the bubbles follow the flow without diffusing as smoke does, the streaklines observed represent the complete time history of individual fluid particles. Therefore details of the horseshoe vortex structure were seen that have never been reported before. Also, end-wall flow directions were observed by using a mixture of oil and a yellow pigment placed as drops on the surface and allowed to flow under the influence of local wall shear stresses.

A motion picture supplement showing the flow visualization results has been prepared and is available from the NASA Lewis Research Center as film supplement C-298. A request card and a description of the film are included at the back of this report.

APPARATUS AND PROCEDURE

Cascade

The cascade contained six vanes that were fabricated to the surface coordinates shown in figure 2. These coordinate values are three times the mean section values of the turbine vanes designed for use in the NASA Lewis High Pressure Turbine Facility (ref. 8). However, the span of the vanes in the test cascade was four times the span of the actual vanes because of a requirement to match the cascade with existing hardware. This change in aspect ratio should not affect the results of the tests since the phenomenon under study is concentrated near the passage end wall. The pertinent cascade parameters were axial chord, 11.4 cm (4.48 in.); ratio of chord to axial chord, 1.46; ratio of pitch to axial chord, 1.08; aspect ratio (ratio of span to axial chord), 1.34; air inlet angle, 0° (axial); air exit angle, 67°.

Airflow through the cascade was drawn in from an atmospheric inlet and exhausted to the laboratory central exhaust system. The wind tunnel built to hold the cascade is shown schematically in figure 3(a). The inlet nozzle was designed for constant acceleration of the flow through it, as described in reference 9. At the end of the inlet nozzle the flow entered a duct 68.6 cm (27 in.) wide by 15.2 cm (6 in.) high by 152.4 cm (60 in.) long. This duct was long enough to ensure a turbulent end-wall boundary layer, as confirmed by profile measurement.

The tunnel boundary layer profile was measured at a point 21.6 cm (8.5 in.) upstream of the vanes. The cascade of six vanes was located at the end of the inlet duct. The end vanes had adjustable tailboards to assure periodicity of the flow through the cascade. One of the vanes in the center of the cascade was instrumented with static pressure taps around the vane at midspan. The cascade inlet Reynolds number, based on true chord, ranged from 1.0×10^5 to 3.0×10^5 for the tests described. From the cascade the flow was ducted to the laboratory central exhaust system. Figure 3(b) shows the cascade test section. The vanes were fabricated from wood and painted black to provide contrast in the photographs. The rest of the cascade was built from clear acrylic plastic, with the bottom end wall painted black.

Flow Visualization Techniques

There was a slot in the end wall located about 21 cm (8.25 in.) upstream of the vane leading edges, as shown in figure 3(a). The helium bubbles used for flow visualization were injected into the boundary layer from a plenum beneath this slot. The bubble-generating system is described in detail in reference 10, and an example of its use for visualization of film cooling is presented in reference 11. Figure 4 shows a cross section of the bubble generator head. The bubble solution flowed through the annulus and was formed into a bubble inflated with the helium passing through the inner concentric tube. The helium-filled bubble was then blown off the tip by a continuous blast of air flowing through the shroud passage. The desired bubble size and neutral buoyancy were achieved by proper adjustment of air, bubble solution, and helium flow rates. As many as 300 bubbles per second could be formed in this device. For these tests the bubble diameter was about 1.5 mm (0.06 in.). The bubble generator head was placed through a grommet in the wall of the plenum beneath the injection slot shown in figure 3(a). The actual rate of bubble injection into the cascade boundary layer was about 13 bubbles per second, as determined by counting bubble streaks on 1-sec photographic exposures of the flow. The reduced rate partly resulted from bubbles in the plenum colliding with the walls and bursting before reaching the injection slot. The number of bubbles entering the horseshoe vortex was further reduced by turbulent fluctuations that carried some bubbles out of the boundary layer and displaced others laterally away from the stagnation region.

The light source for bubble illumination consisted of a 300-W quartz arc lamp, a rectangular aperture, and a 300-mm lens. The light source was located upstream of the tunnel inlet nozzle and projected a beam down the tunnel into the cascade. The image of the aperture was focused in the cascade, and its vertical location was adjustable to illuminate either the boundary layer or the free stream. When viewed from above, or from the side, the bubbles showed up very brightly when they were in the light beam. Photographs of the bubbles were taken from two locations: directly above the cascade, providing a plan view of the flow; and upstream of the cascade, looking through the tunnel side wall into the cascade, providing an oblique view of the flow. At both locations a motion picture camera, running at either 3 or 12 frames per second, was used to record the bubble traces. Also, for the plan view, a series of 1-sec time exposures were taken with a

35-mm still camera. The motion pictures that were taken have to be considered as a collection of independent data records, since the time of flight of the bubbles through the field of view was much shorter than the open time of the shutter. Thus the bubbles appear as streaklines on the film, and adjacent frames of the film can never show the same bubble. The combination of low bubble injection rate, boundary layer turbulence, and camera shutter speed resulted in only about one film frame in every 100 containing something of interest. The procedure was to view the film, one frame at a time, and make 35-mm negatives of the interesting frames.

A second technique used to visualize the flow was to inject smoke into the stream through a probe. A smoke generator was constructed, similar to that described in reference 5; it is shown schematically in figure 5. The source of the smoke was a burning, oil-soaked cigar. A regulated air supply provided combustion air. The smoke was carried through a trap to allow large oil droplets to settle out; then it was ducted to the test section. Smoke flow rate to the probe was adjusted by varying the bleed valve shown in figure 5. The same lighting and camera system was used for the smoke as was used for the bubbles. The smoke had the advantage that it could be precisely placed where desired, but the disadvantage was that it diffused and, being a continuous source, tended to average out temporal variations in the flow. This means that local details of the horseshoe vortex cannot be observed with smoke, but it does a good job of delineating regions of the flow and showing gross fluid motions.

Additionally drops of oil, mixed with a yellow pigment, were placed on the end wall and began to flow when the tunnel was run. The smeared-out drops were then photographed, presenting a view of limiting streamlines on the surface.

Vortex Modification Technique

Reference 7 showed that end-wall secondary flow aerodynamic losses were reduced when film cooling holes on the end wall were aligned such that the jet flows tended to impede the secondary flows. These positive results suggested a possible way to control the horseshoe vortex by injecting air into the region where the vortex originates. To investigate this, a number of control jet holes were drilled in the end wall near the vane leading edge. A total of 17 holes were added, layed out as shown in figure 6 around the two vanes in the middle of the cascade. These holes were drilled at an angle of 15° to the surface, exiting in the axial direction, aimed downstream. The supply tube to each hole was capped so they could be tested one at a time. The test procedure was to uncap the desired test jet, connect it to a metered air supply through a ball valve, and photograph the effect on smoke entrained in the horseshoe vortex when the control jet ball valve was opened. The smoke for these tests was injected into the flow on the leading edge of the vane near the end wall. With the control jet off the smoke followed a path down the leading edge to the end wall, then moved upstream in the region behind the separation line, and finally turned and flowed downstream in the horseshoe vortex. An indicator light visible to the camera indicated whether the jet was on or off. The control jet layout was selected to provide jets both upstream of and directly under the horseshoe vortex, close to the leading edge.

RESULTS AND DISCUSSION

Cascade Aerodynamics

The cascade was run over a range of inlet Reynolds number, based on true chord, of 1.0×10^5 to 3.0×10^5, corresponding to a tunnel inlet velocity range of 9.4 m/sec (31.0 ft/sec) to 28.6 m/sec (94.0 ft/sec). Because over this range of velocity no change was observed in the behavior of the horseshoe vortex, it was decided to run at the lower velocity for all data photographs, since the slower bubbles were easier to photograph and smoke diffusion was minimized. Periodicity of the cascade was set by monitoring the end-wall static pressures in the center of each passage at the cascade exit and then adjusting the tailboards. Figure 7 shows the pressures measured, for two different velocity levels, after final setting of the tailboards. The pressures are referenced to atmospheric.

To quantify the flow field through the cascade, measurements were made of the static pressure distribution around one of the vanes at midspan. Figure 8 gives the results of one set of measurements. For the run shown, total pressure was 98.4 kPa (14.27 psia), free-stream total temperature was 297 K (75° F), tunnel velocity upstream of the cascade was 29 m/sec (95.3 ft/sec), and exit Mach number was about 0.21. These conditions represent the maximum flow rate used in the facility. The error bars in figure 8 represent the range of data over eight readings.

The velocity profile through the end-wall boundary layer was surveyed with a total pressure probe at a point 1.9 axial chords upstream of the vanes. The dimensionless profile is shown in figure 9. For this run, total pressure was 100 kPa (14.5 psia), free-stream total temperature was 299 K (78° F), and tunnel velocity was 13.1 m/sec (43 ft/sec). Also included in figure 9 is the logarithmic distribution in the wall region for a fully turbulent boundary layer (ref. 12). The boundary layer thickness, defined as the point where the velocity is 99 percent of the free-stream value, was 1.81 cm (0.714 in.). Momentum thickness was 0.165 cm (0.065 in.) and the boundary layer shape factor was 1.27. Momentum thickness Reynolds number was 1389. These values are as would be expected for an equilibrium turbulent boundary layer.

Boundary Flow Directions

The flow directions along the end-wall surface are discussed first. Figure 10 is a representative plan view photograph of oil drop traces observed in these tests. The location of the separation saddle point is indicated in the figure. Because this cascade had a smaller turning angle than the one in reference 4, and thus a milder pressure gradient across the passage, the saddle point was much closer to the vane than shown for the blades in reference 4. The separation line that crossed the passage from the saddle point to the suction side of the adjacent vane reached that vane surface at about 50 percent of axial chord. At that location the oil streaks were observed to flow up the suction surface and curve back toward the trailing edge. Near the cascade exit the end-wall oil streaks flowed directly across the passage in a tangential direction, from the pressure side to the suction side. The end-wall oil traces in the wake region behind the vane trailing-edge region followed the vane exit angle smoothly, further indicating good periodicity for the cascade. Comparison of the end-wall

flow traces of this work with that of Marchal and Sieverding (ref. 6), who used a vane of similar profile, shows good agreement.

Additional details of the separation saddle point are shown in figure 11. Figure 11 consists of tracings from photographs of the path followed by smoke allowed to enter the boundary layer through the vortex control jet holes. The grid superimposed on figure 11 is made up of 2.54-cm (1-in.) squares. The observed smoke paths correlate well with the oil drop traces in figure 10.

The end-wall traces just discussed provide a visible boundary condition on the three-dimensional secondary flows. At the other extreme, outside the boundary layer, the free-stream potential flow solution provides the limit. To visualize the free-stream flow, a fine stream of smoke was introduced into the flow at a distance above the end wall sufficient to insure that it was out of the boundary layer. Figure 12 illustrates schematically the flow direction approaching the cascade and the direction of illumination used for the free-stream smoke tests of figure 13. The camera was mounted directly over the middle passage of the cascade, looking straight down, giving a plan view of the flow. The lamp was mounted at the location identified as the "alternative light source" in figure 3(a). This resulted in a pattern of shadows on the photographs as outlined in figure 12. Note that most of the pressure surface was in shadow for these figures and that smoke or bubbles in the shadowed regions thus are not visible. This same lighting configuration was used for the boundary layer smoke and helium bubble tests described in the next section. The free-stream smoke flow results are shown in figure 13. Four different smoke traces are presented in figures 13(a) to (d). The smooth paths followed by the smoke are indicative of the flow outside the boundary layer. Note in figure 13(d) that smoke input along a stagnation streamline flowed to the vane leading edge and smoothly split between the suction and pressure sides. The smoke to the pressure side in figure 13(d) disappeared into the shadow of the leading edge.

With both the end-wall and freestream-flow directions thus delineated, attention was turned to the region of flow situated between these two extremes.

Horseshoe Vortex Visualization

Figures 14 and 15 show some details of the horseshoe vortex and end-wall secondary flows. The camera position and lighting angle were the same in these figures as shown in figure 12. The only difference in lighting was the distance of the light beam above the end-wall surface. In figures 14 and 15 the beam was a sheet of light, approximately 0.95 cm (0.375 in.) thick, grazing the end wall; in figure 13 the beam was located above the end wall, illuminating the free stream. Dirt and dust particles on the surface show up in the photographs as bright dots against the black background of the end wall. Near the cascade exit, beam divergence caused large reflections from the end wall, making it difficult to trace the smoke or bubbles beyond the exit. The grid superimposed on the photographs is made up of 2.54-cm (1-in.) squares.

Figures 14(a) to (e) show what happens to smoke injected into the boundary layer upstream of the cascade. In figures 14(a) to (d) the probe tip was close to the end-wall surface and is shown at four successive locations. In figures 14(a) and (b) the smoke was injected along a streamline to the right of the stagnation streamline. The smoke was quickly deflected

further to the right as it encountered the horseshoe vortex pressure-side leg, remaining on the upstream side of the separation line shown in figure 10. Comparison of figures 14(a) and (b) with figure 13(c) shows a marked difference between the paths taken by free-stream smoke and end-wall boundary layer smoke.

Figures 14(c) and (d) show the behavior of smoke injected into the boundary layer along a stagnation streamline. Comparing these figures with figure 13(d) shows that there are major differences. In the boundary layer the smoke near the end wall never reached the vane leading edge but stagnated ahead of it and split to both sides, leaving a clear region in front of the vane. Figure 14(e) gives an indication of where the fluid comes from to fill this clear region. In this figure the smoke probe was raised slightly but was kept aligned with the stagnation streamline. The smoke carried all the way to the vane leading edge, at which point it curled down toward the end wall and back upstream, filling what was the clear region in figure 14(d) with smoke. This smoke was caught in the horseshoe vortex.

The difficulty with using smoke is evident in figure 14. Details of the flow are not apparent because each smoke particle behaves as an individual fluid particle and the paths traced by the many particles in the smoke cloud merge to a blur on the photographs. On the other hand, the neutrally buoyant bubbles represent discrete fluid volumes, and their rate of injection is low enough that the paths followed by these individual volumes are clearly revealed on the photographs.

In figure 15, a selection of frames from the motion picture data showing bubble streaklines are presented, with a grid overlay, to show the extent and behavior of the horseshoe vortex. To aid in interpreting figure 15, recall that the time for a bubble to pass through the cascade was shorter than the time that the camera shutter was open. Thus the light reflected from the bubble showed as a streak on the film. Also, the bubbles were randomly spaced in time, so that when the shutter opened or closed, a bubble might be part way through the passage. The result was a streak that appears to start or stop somewhere in the passage other than at the edges of the illuminated region as diagrammed in figure 12. Before looking in detail at figure 15, a look back at figure 11 to locate the position of the separation saddle point will aid in interpreting the bubble streaklines.

The bubbles caught in the horseshoe vortex show as wavy streaklines in the photographs in figure 15. This wavy appearance is actually the plan view of a bubble following a corkscrew-like path through the cascade. The emphasis in figure 15 is on bubbles in the pressure-side leg of the vortex because the suction-side leg of the vortex was held close to the end-wall - vane corner by the secondary flows and the pressure gradient, and the bubbles were too large to survive in this region close to the surface.

Figures 15(a) to (c) illustrate that only a small fraction of the boundary layer flow got caught in the horseshoe vortex. For the conditions shown the boundary layer thickness was about 1.8 cm (0.71 in.), but the light sheet was only 0.95 cm (0.375 in.) high. Still, some bubbles showed no indication of being affected by the horseshoe vortex, even though they were obviously in the boundary layer. One trace in each of figures 15(a) to (c) followed a path that appears to be like the free-stream smoke traces in figure 13.

Figures 15(d) to (k) are included to show the variation observed in the paths followed by bubbles in the horseshoe vortex. Figure 15(d) shows a bubble executing at least three complete loops in a very short distance, about 2.54 cm (1 in.), before it disappears from view, probably because the

shutter closed at that time. Figures 15(e) and (f) also show tight loops over short distances. These bubbles appear to be caught very close to the vortex core. In figures 15(g) to (k) bubbles show paths that are progressively smoother, representing bubbles caught in the outer part of the vortex.

Note that in all cases shown in figure 15, the path of the vortex lay on the downstream side of the saddle point and the separation line shown by the oil drop traces in figure 10. Near the leading edge the vortex path closely followed the end-wall-limiting flow directions, but further down the passage there was a big difference in direction between the two, as the vortex core appeared to remain near the middle of the passage rather than to continue to the suction-side corner. This is the same type of behavior as noted for the stator cascade in reference 6. The fact that the vortex location in the stator cascade was markedly different than that observed in a rotor cascade implies that the heat transfer patterns on the end wall will also be different. Some additional evidence of this is provided when the work of Georgiou et al. (ref. 13) is compared with that of Graziani et al. (ref. 3). Georgiou et al. (ref. 13) reported iso-heat-transfer lines for a stator cascade similar to the one used by Marchal and Sieverding (ref. 6). In their work (ref. 13), the location of the maximum end-wall heat flux near the cascade exit appeared to be near the middle of the passage; in reference 3 it appeared to be closer to the suction surface.

A more vivid picture of the paths followed by bubbles trapped in the horseshoe vortex is presented in the next series of photographs. For the photographs in this series the camera was moved to the side of the tunnel, about the location marked "alternative light source" in figure 3(a). The angle of the camera was adjusted to give an oblique view of the cascade and focused on just one passage. For this series the lamp was moved to the upstream position so that the light beam was projected axially down the tunnel as diagrammed in figure 16. Figures 17(a) and (b) were taken from the part of the motion pictures with the room lights still on to further aid in orienting the observer. Note the height of the light beam where it hit the vane surfaces in figure 17(b) and the reflections off the end wall. Also visible in figure 17(b) is a bubble streakline, with the reflection of the streakline faintly visible on the end wall. The straight line in figures 17(a) and (b), seen as rising from left to right behind the vanes, marks the intersection of the left tailboard (fig. 3(a)) and the end wall. The remaining parts of figure 17 show the streaklines of bubbles flying through the passage and responding to the horseshoe vortex. Comparing different streaklines revealed that those closest to the surface initially, as deduced from their reflections, followed a tighter corkscrew-like path than those initially farthest from the end wall.

Modification Tests

Some of the results of the attempts to modify the horseshoe vortex are shown in figure 18. The hole numbers are as shown in figure 6. Figure 18 consists of pairs of photographs of smoke in the horseshoe vortex with the control jet off and with the control jet on, for all the holes for which there was a noticeable effect. In all cases, the time difference between the jet-off and jet-on views for a given control jet was less than half a second. For these runs the smoke was put in at the vane leading edge so that it flowed down to the end wall, where it was caught in the vortex rollup. Note that the path of the vortex, as delineated by the smoke, moved

closer to the vane pressure side when the control jet was turned on (as indicated by the glowing indicator light). The effect was very pronounced for the control jets located near the saddle point (figs. 18(e) to (h), (k) and (l), and (s) and (t)), and appeared to diminish for jets away from the saddle point.

The flow rate to a control jet was varied to determine the minimum blowing rate required to see the effect. It was observed that below a jet - free-stream velocity ratio of about 1.5, there was no deflection of the smoke in the vortex. This blowing rate was considerably higher than that which would normally be available in an engine, so the use of a single jet to modify the horseshoe vortex may not be practical. However, since a definite effect on the horseshoe vortex was demonstrated, further research on the phenomenon is warranted, particularly on the effect of multiple control jets.

CONCLUDING REMARKS

Streakline flow visualization with neutrally buoyant bubbles was used in conjunction with end-wall oil flow traces to show details of the development of the horseshoe vortex and the subsequent passage vortex in a two-dimensional dimensional turbine stator cascade. Plan view pictures of the bubble streaklines and oblique, perspective views show that the fluid closest to the wall in the inlet boundary layer rolled up to form a tight vortex core. Fluid from farther out in the boundary layer was entrained in this vortex. Comparison of the bubble streaklines with oil flow traces on the end wall shows that the path of the vortex was aligned more with the free-stream flow than with the end-wall-limiting flow. Near the trailing edge the vortex core was observed to be about midway between the pressure and suction sides of the passage.

SUMMARY OF RESULTS

A flow visualization study has been conducted to examine details of the horseshoe vortex formed by the rollup of the turbulent end-wall boundary layer in a large-scale, two-dimensional turbine stator cascade. Included in the study were attempts to modify the vortex structure by using control jets.

Flow visualization was accomplished by using both small, neutrally buoyant helium-filled soap bubbles and smoke from oil-soaked cigars. The smoke provided a time-averaged glimpse of the vortex, while the bubbles revealed the actual streamlines, appearing as streaks on photographs.

The effectiveness of individual control jets, located on the end wall near the vane leading edge, was investigated by observing the changes in smoke flow patterns when the control jets were cycled on and off, one at a time. Results of the investigation are as follows:

1. Results of the smoke flow tests showed that the fluid in the boundary layer closest to the end wall, near the stagnation streamline, was deflected away from the vane leading edge by the horseshoe vortex secondary flows. Smoke injected into the outer regions of the boundary layer along a stagnation streamline was observed to reach the vane leading edge, curl down to the end wall, and flow forward along the end wall a short distance before turning in a downstream direction and becoming entrained in the horseshoe vortex.

2. Neutrally buoyant helium-filled bubbles were injected into the end-wall boundary layer upstream of the vanes, and the paths they followed were recorded as streaks on photographs. Those bubbles that approached the vane leading edge close to the end wall and along the stagnation streamline were observed to follow a violently twisting path as they entered the horseshoe vortex and then to corkscrew downstream along the path of the vortex. Other bubbles close to the stagnation streamline, farther from the end wall but still in the boundary layer, were observed to follow the same general path but with fewer twists. Bubbles in the boundary layer but well off the stagnation streamline were deflected by the horseshoe vortex in the passage but did not appear to be entrained in the vortex itself.

3. A preliminary attempt was made to modify the horseshoe vortex by injecting high-energy air through control jets on the end wall near the vane leading edge. Seventeen different jet locations were investigated. The procedure was to introduce smoke into the horeshoe vortex and photograph the flow pattern with individual control jets cycling off and on. The jets were tested one at a time. The results showed that some of the jets had a marked effect on the observed smoke flow patterns. Smoke that was in the vortex jumped back and followed a path close to the vane surface when a particular control jet was activated. The jets that seemed to have the biggest effect were those blowing into the region near the end-wall separation saddle point. Variation of control jet flow rate indicated that a minimum jet - free-stream mass velocity ratio of about 1.5 was required to bring about an observable effect. Quite often this region must be film cooled. It appears that it may be possible to use film cooling jets to favorably affect the horseshoe vortex.

Lewis Research Center
National Aeronautics and Space Administration
Cleveland, Ohio, January 18, 1982

REFERENCES

1. Graham, R. W.: Fundamental Mechanisms That Influence the Estimate of Heat Transfer to Gas Turbine Blades. ASME Paper 79-HT-43, Aug. 1979.
2. Blair, M. F.: An Experimental Study of Heat Transfer and Film Cooling on Large-Scale Turbine Endwalls. J. Heat Transfer, vol. 96, no. 4, Nov. 1974, pp. 524-529.
3. Graziani, R. A.; et al.: An Experimental Study of Endwall and Airfoil Surface Heat Transfer in a Large Scale Turbine Blade Cascade. ASME Paper 79-GT-99, Mar. 1979.
4. Langston, L. S.; Nice, M. L.; and Hooper, R. M.: Three-Dimensional Flow Within a Turbine Cascade Passage. J. Eng. Power, vol. 99, no.1, Jan. 1977, pp. 21-28.
5. Herzig, Howard Z.; Hansen, Arthur G.; and Costello, George R.: A Visualization Study of Secondary Flows in Cascades. NACA TR-1163, 1954.
6. Marchal, P.; and Sieverding, C. H.: Secondary Flows Within Turbomachinery Bladings. Secondary Flows in Turbomachines. AGARD CP-214, 1977, pp. 11-1 - 11-20.
7. Goldman, L. J.; and McLallin, K. L.: Effect of Endwall Cooling on Secondary Flows in Turbine Stator Vanes. Secondary Flows in Turbomachines. AGARD CP-214, 1977, pp. 15-1 - 15-29.

8. Szanca, Edward M.; Schum, Harold J.; and Hotz, Glen M.: Research Turbine for High-Temperature Core Engine Application. I - Cold-Air Overall Performance of Solid Scaled Turbine. NASA TN D-7557, 1974.
9. Yuska, Joseph A.; Diedrich, James H.; and Clough, Nestor: Lewis 9- by 15-Foot V/STOL Wind Tunnel. NASA TM X-2305, 1971.
10. Hale, R. W.; et al.: Development of Integrated System for Flow Visualization in Air Using Neutrally Buoyant Bubbles. SAI-RR-7107, Sage Action, Inc., 1971. (AD-756691).
11. Colladay, Raymond S.; and Russell, Louis M.: Streakline Flow Visualization of Discrete-Hole Film Cooling with Normal, Slanted, and Compound Angle Injection. NASA TN D-8248, 1976.
12. Schlichting, Hermann: Boundary-Layer Theory. Sixth ed., McGraw-Hill, 1968.
13. Georgiou, D. P.; Godard, M.; and Richards, B. E.: Experimental Study of the Iso-Heat-Transfer-Rate Lines on the End-Wall of a Turbine Cascade. ASME Paper 79-GT-20, Mar. 1979.

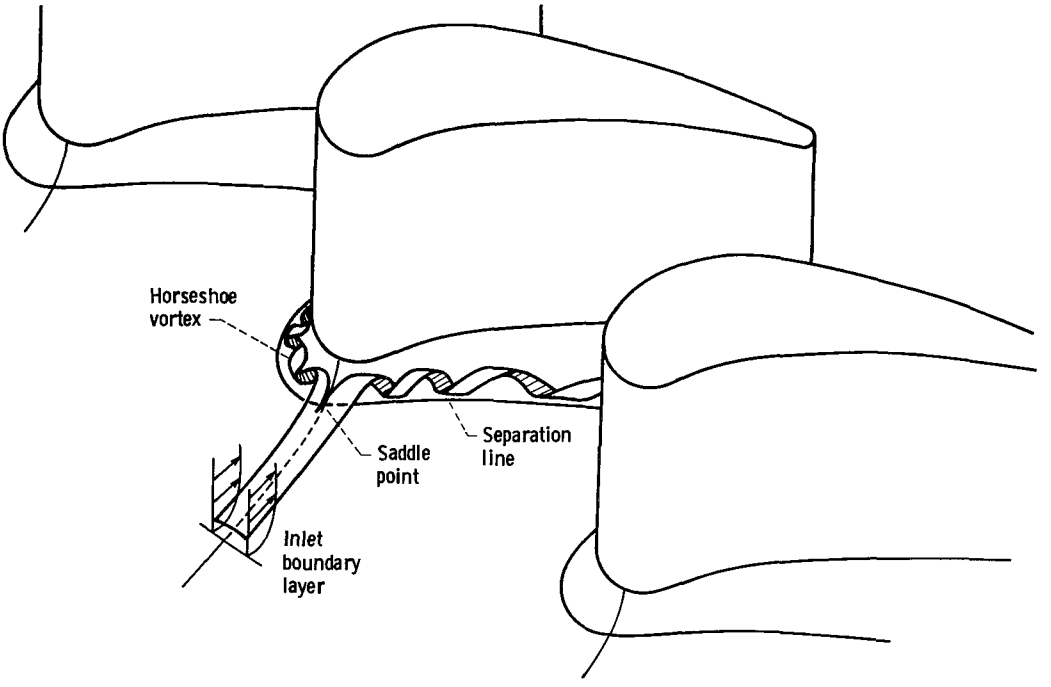

Figure 1. - Schematic representation of end-wall boundary layer rollup into a horseshoe vortex.

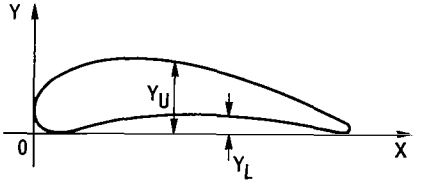

X		Y_L		Y_U	
cm	in.	cm	in.	cm	in.
0	0	1.524	0.600	1.524	0.600
.305	.120	.610	.240	2.438	.960
.381	.150	.518	.204	2.553	1.005
.762	.300	.206	.081	3.018	1.188
1.143	0.450	0.046	0.018	3.368	1.326
1.524	.600	0	0	3.642	1.434
1.905	.750	.046	.018	3.863	1.521
2.286	.900	.191	.075	4.039	1.590
2.667	1.050	0.358	0.141	4.176	1.644
3.048	1.200	.495	.195	4.282	1.686
3.429	1.350	.617	.243	4.359	1.716
3.810	1.500	.724	.285	4.404	1.734
4.191	1.650	0.800	0.315	4.420	1.740
4.572	1.800	.876	.345	4.427	1.743
5.334	2.100	.991	.390	4.389	1.728
6.858	2.700	1.118	.440	4.145	1.632
8.382	3.300	1.143	0.450	3.772	1.485
9.906	3.900	1.059	.417	3.330	1.311
11.430	4.500	.891	.351	2.835	1.116
12.954	5.100	.663	.261	2.240	.882
14.478	5.700	0.396	0.156	1.554	0.612
16.002	6.300	.076	.030	.777	.306
16.657	6.558	.267	.105	.267	.105

Figure 2. - Vane coordinates.

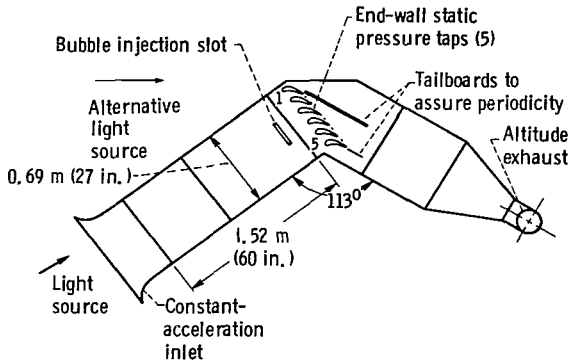

(a) Schematic plan view; tunnel height, 0.15 m (6 in.)

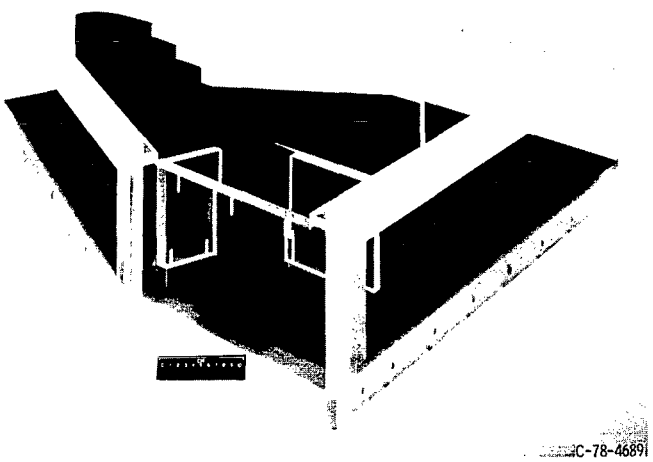

(b) Cascade test section.

Figure 3. - Flow visualization rig.

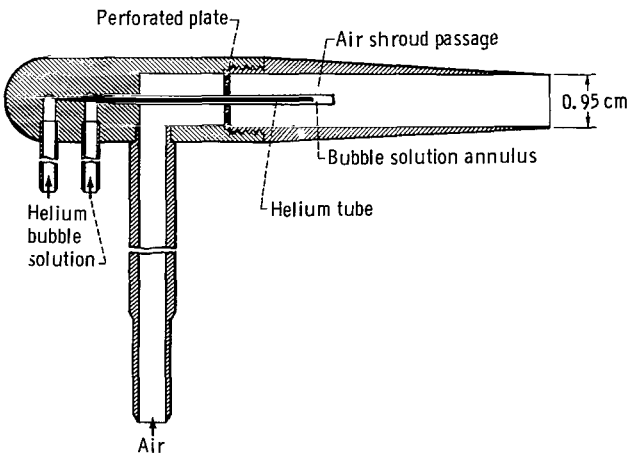

Figure 4. - Bubble generator head.

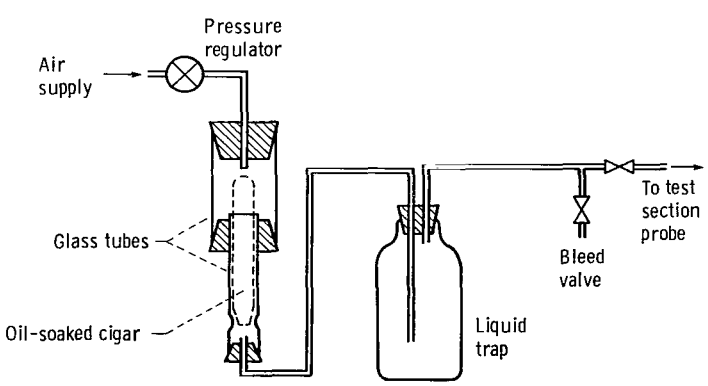

Figure 5. - Cigar smoke generator.

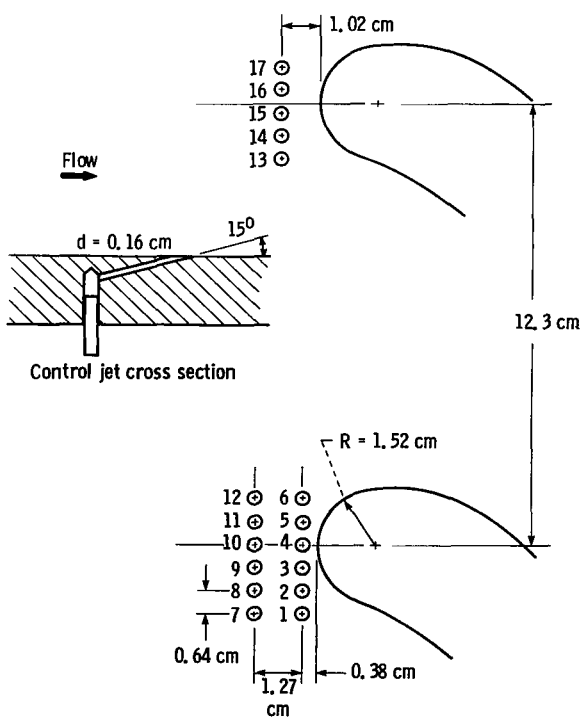

Figure 6. - Distribution of control jet holes.

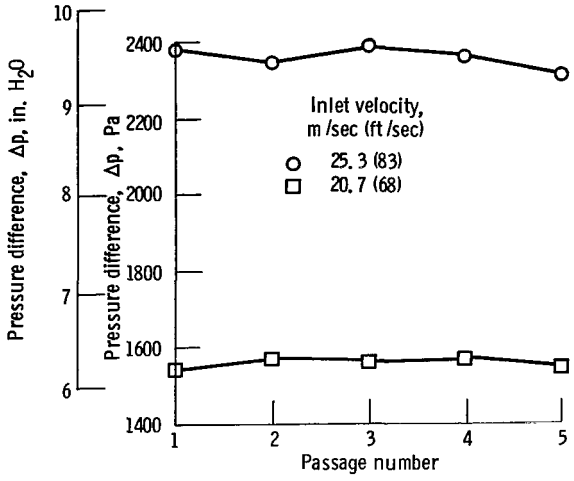

Figure 7. - Cascade periodicity.

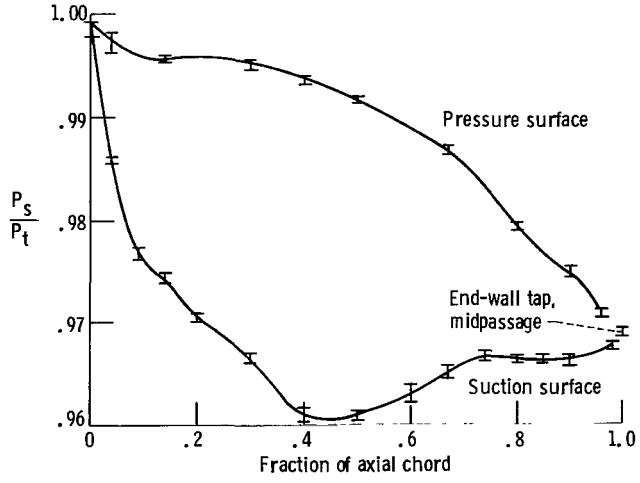

Figure 8. - Pressure distribution measured around vane.

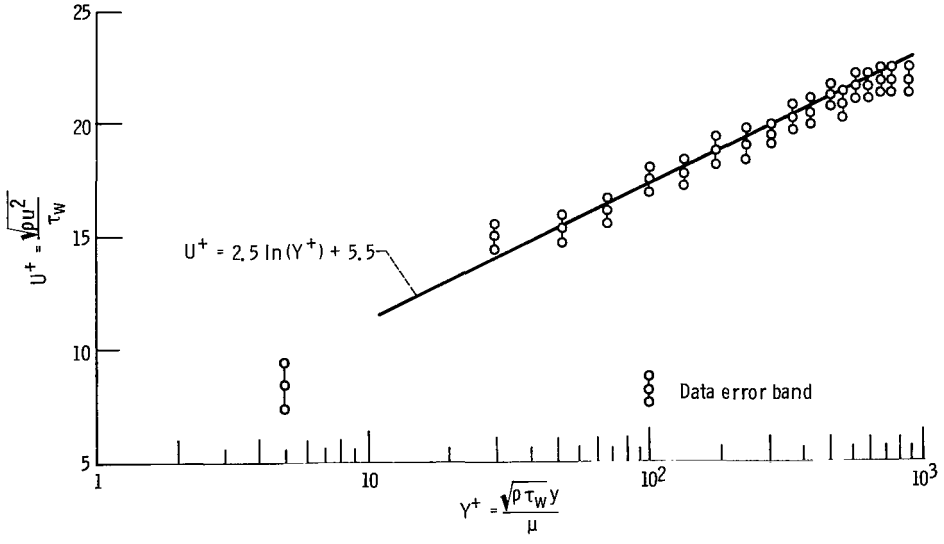

Figure 9. - Boundary layer profile at entrance to vanes, where ρ denotes density, μ denotes viscosity, u denotes velocity, τ_w denotes shear stress at wall, and y denotes distance from wall.

Figure 10. - End-wall oil traces.

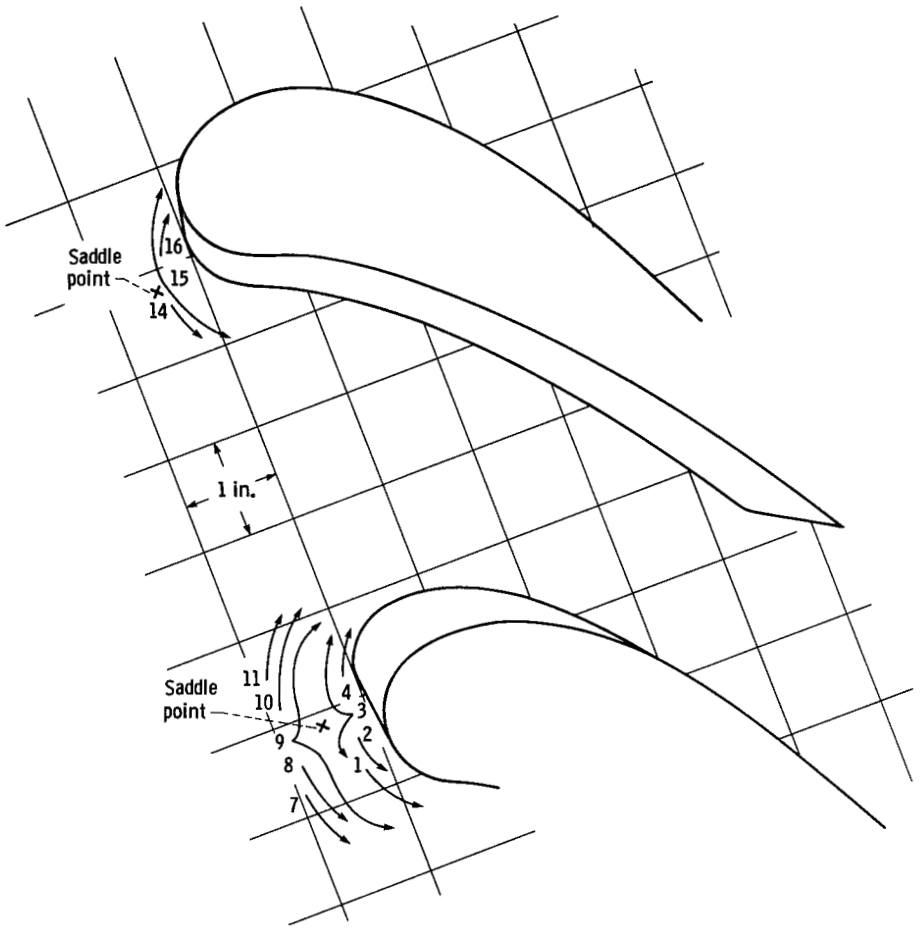

Figure 11. - Saddle point location determined by smoke flow, smoke in vortex control jet holes.

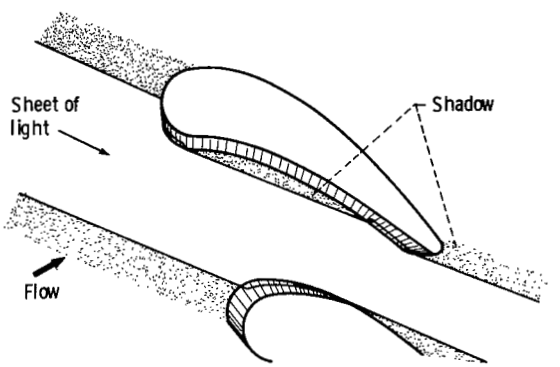

Figure 12. - Region of illumination for figures 13, 14, and 15.

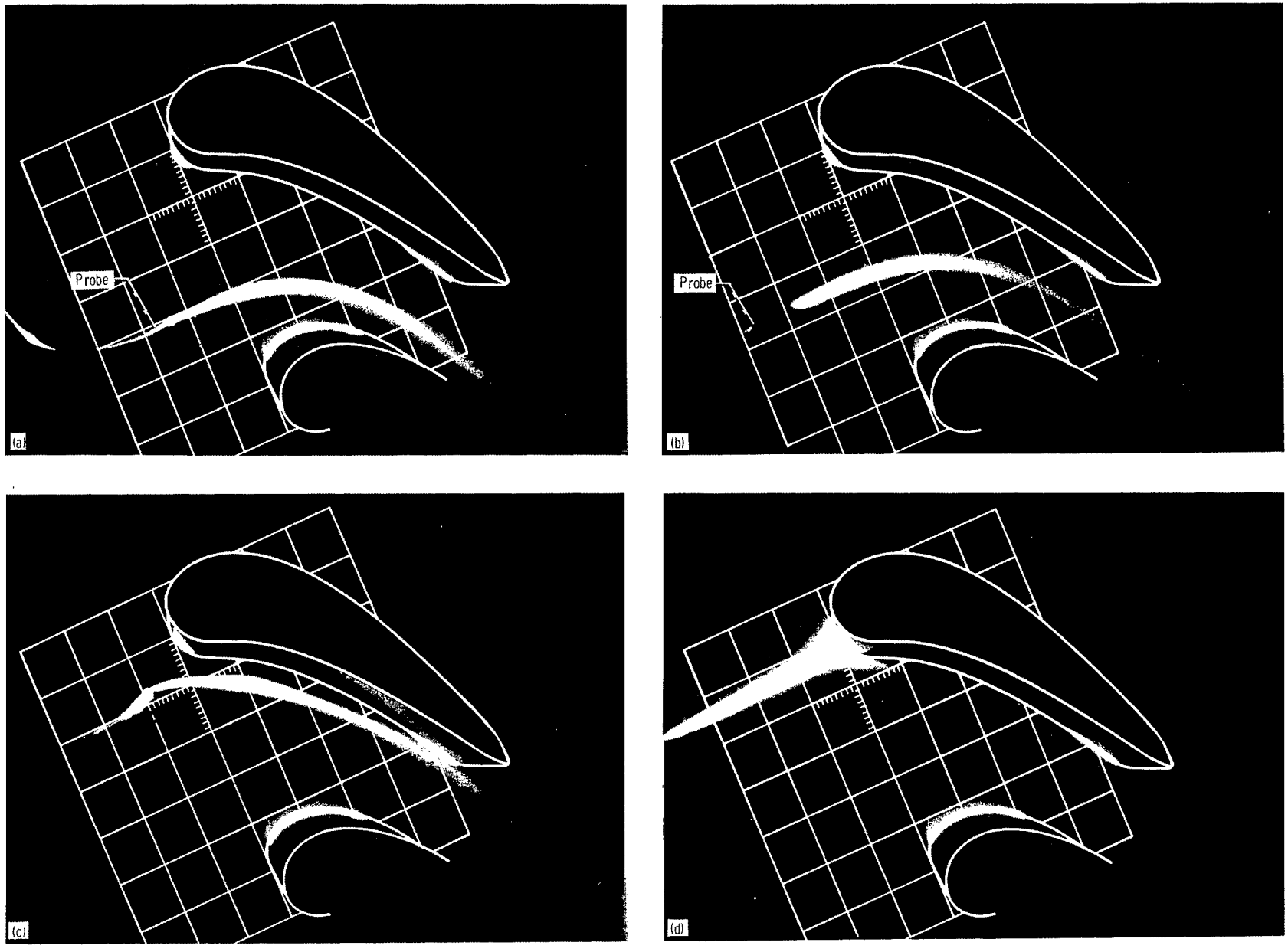

Figure 13. - Smoke in free stream, outside boundary layer.

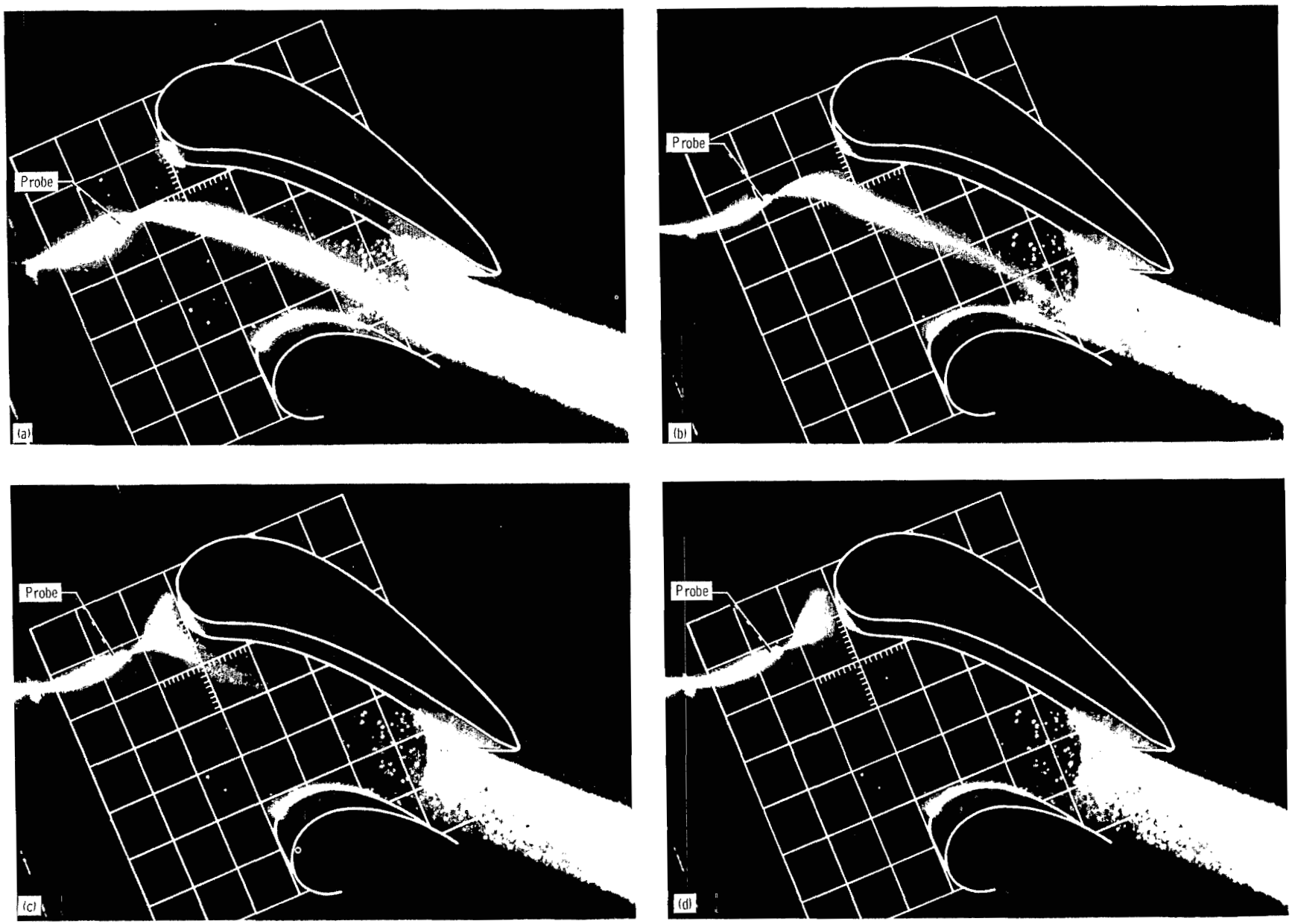

Figure 14. - Smoke injected in boundary layer.

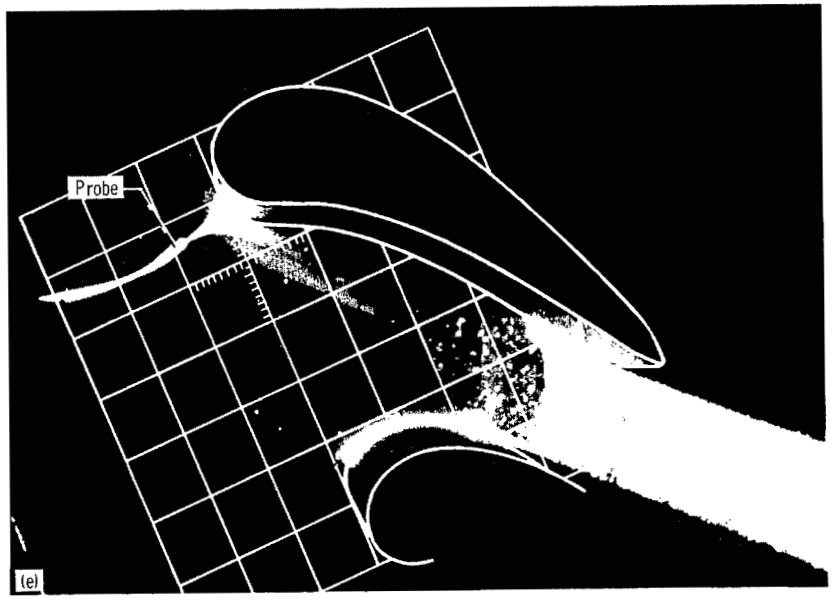

Figure 14. - Concluded.

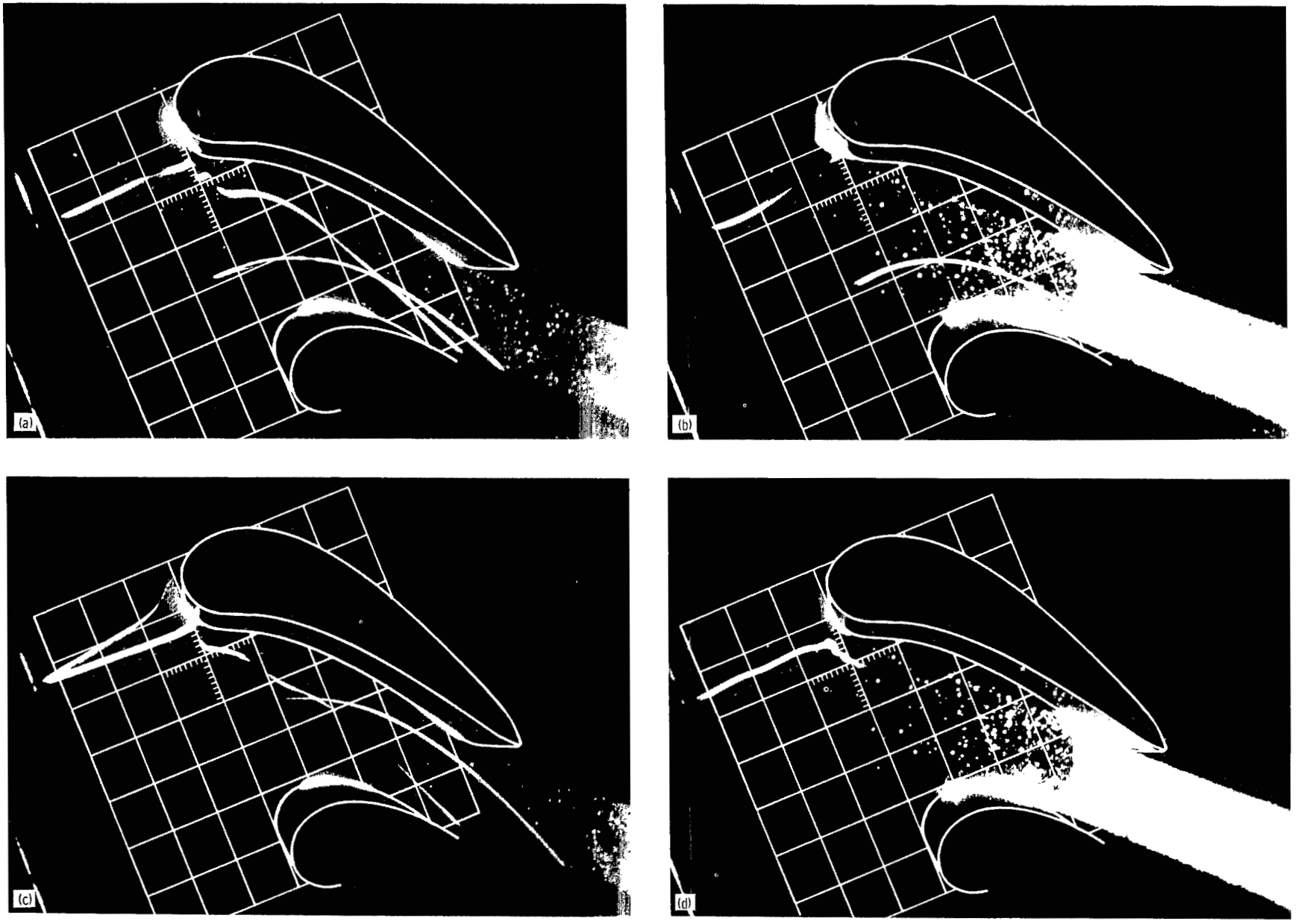

Figure 15. - Bubble streaklines, plan view.

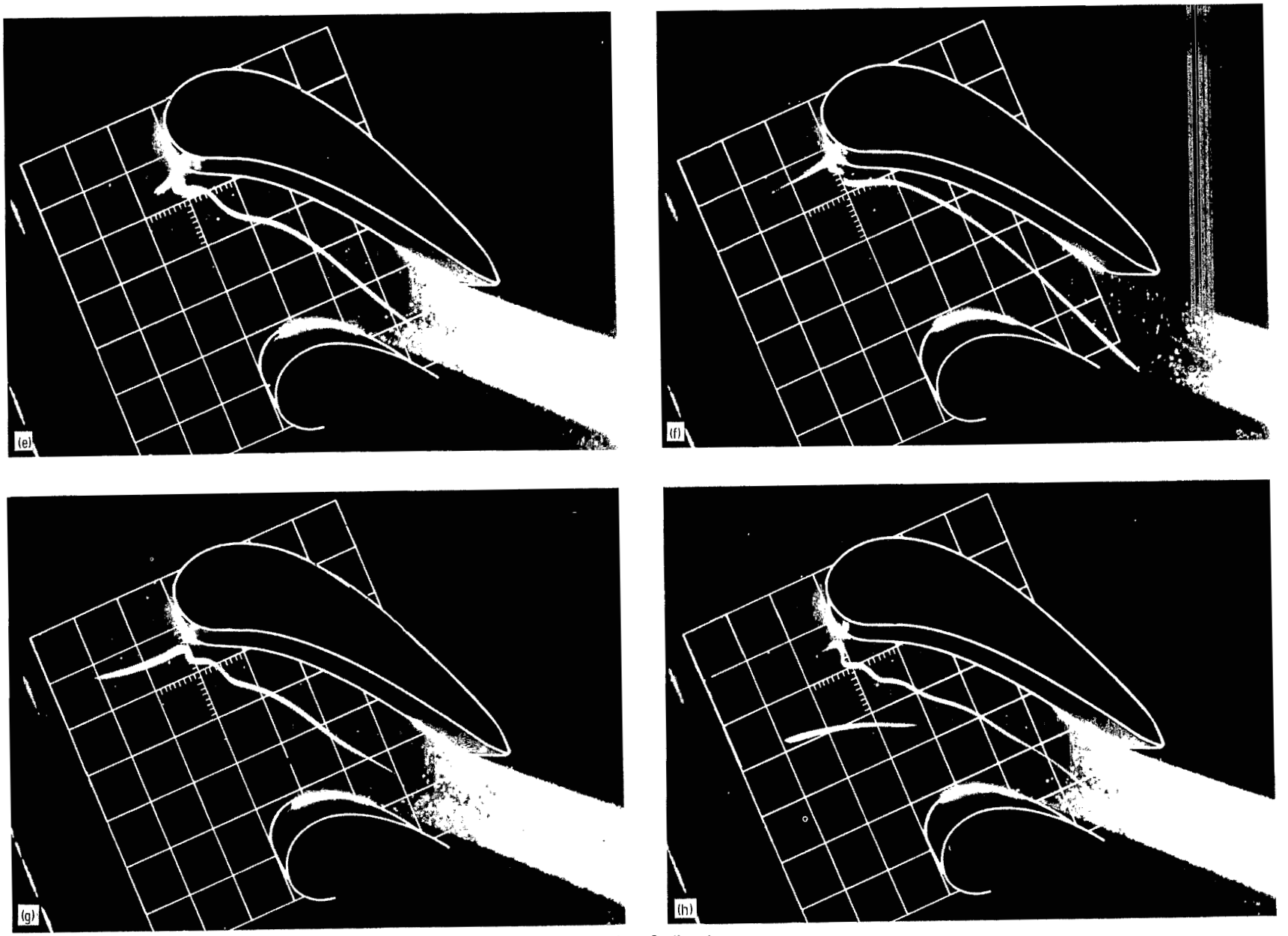

Figure 15. - Continued.

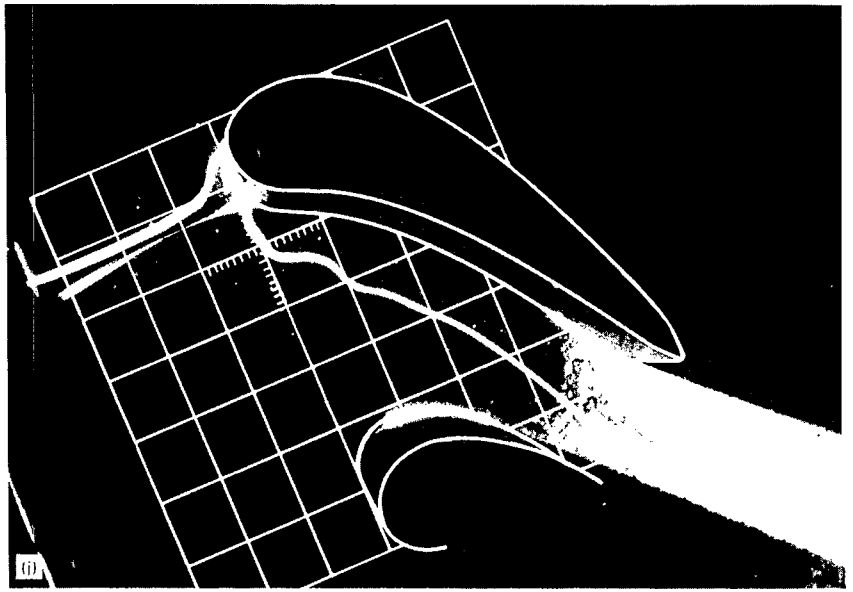

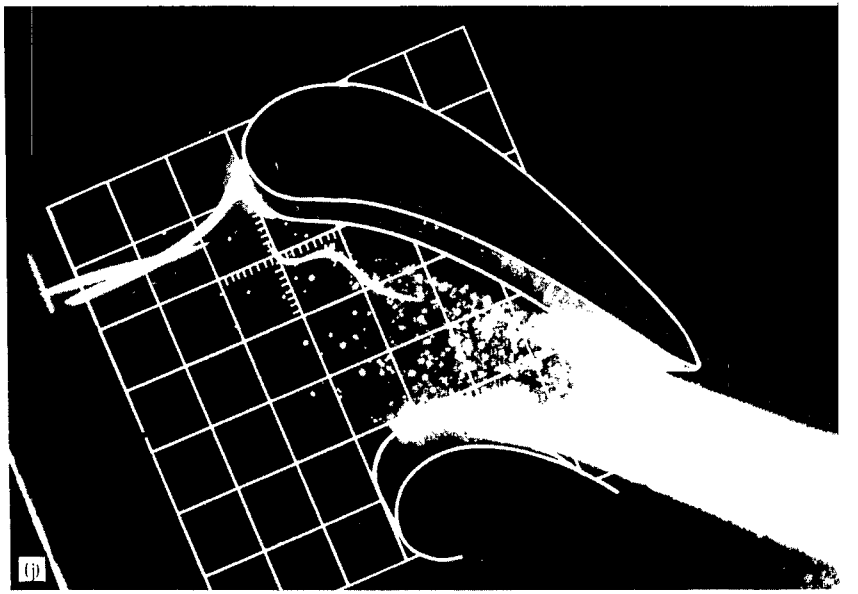

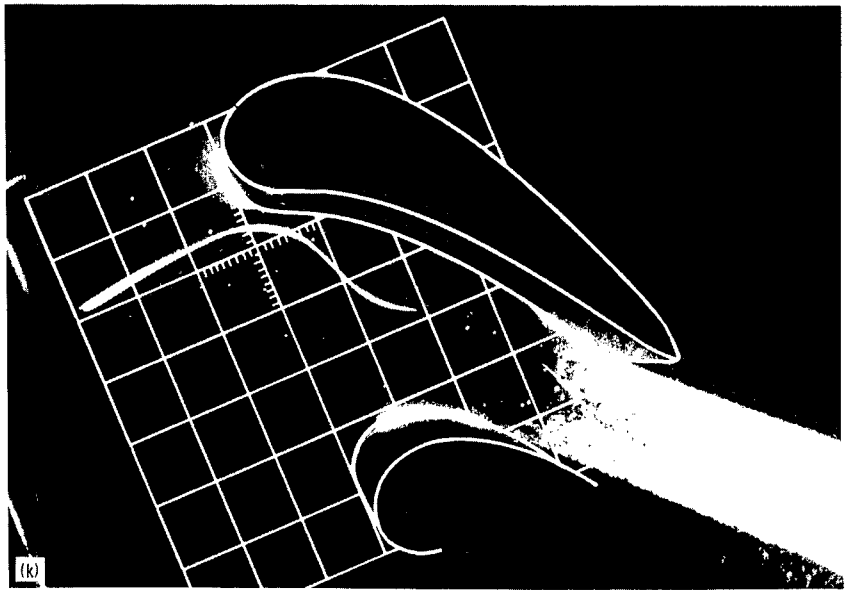

Figure 15. - Concluded.

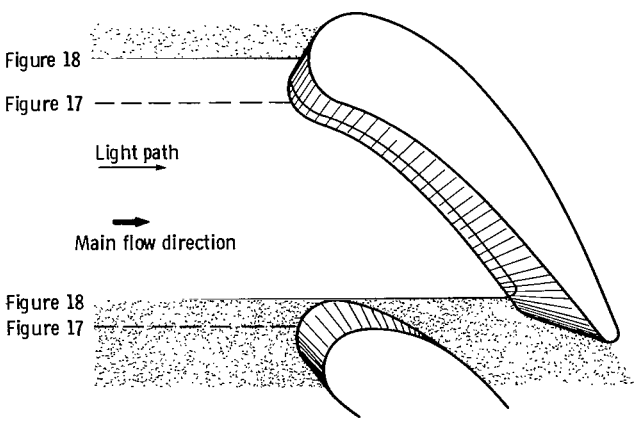

Figure 16. - Region of illumination for figures 17 and 18.

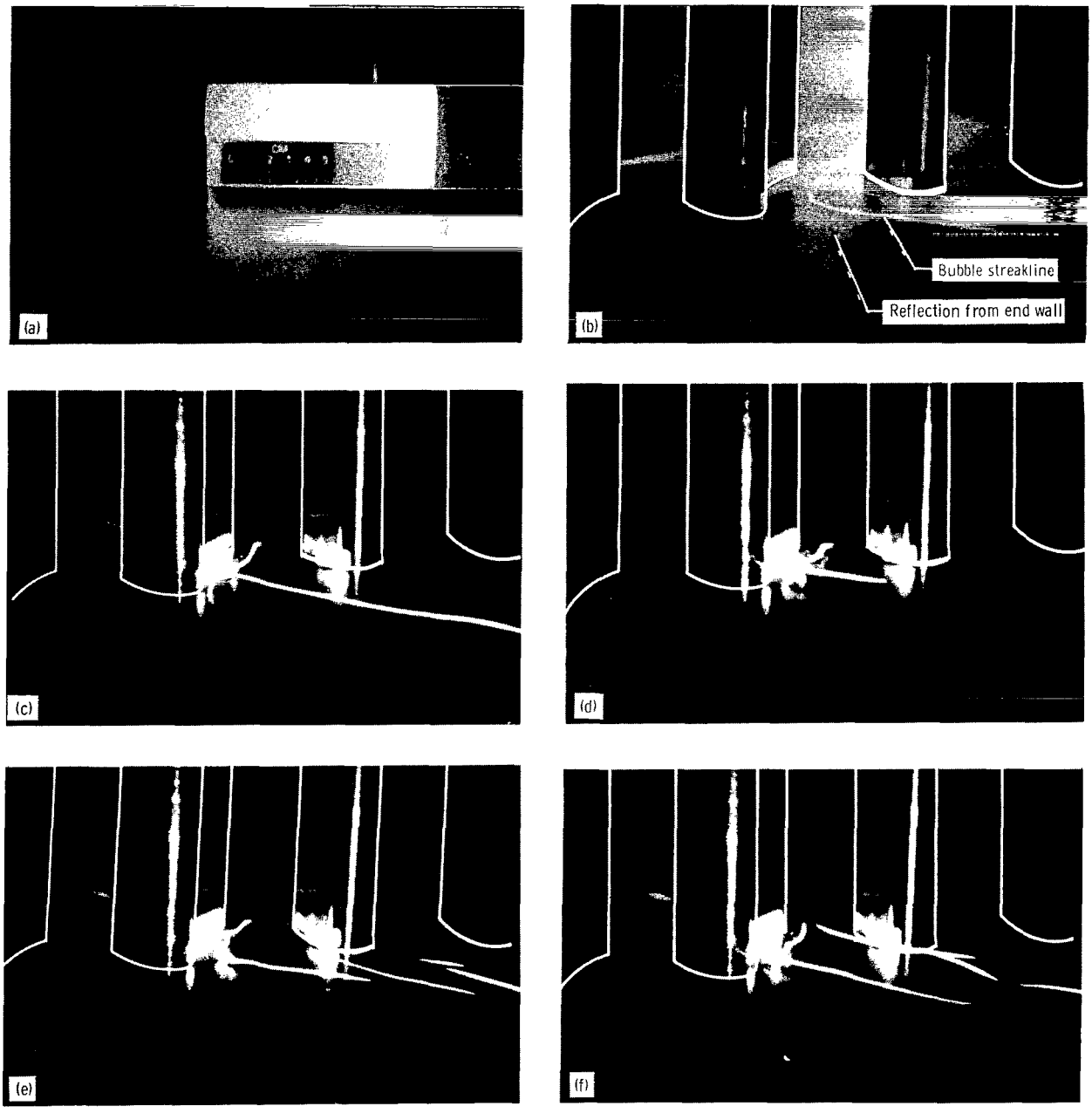

Figure 17. - Oblique view of bubble streaklines.

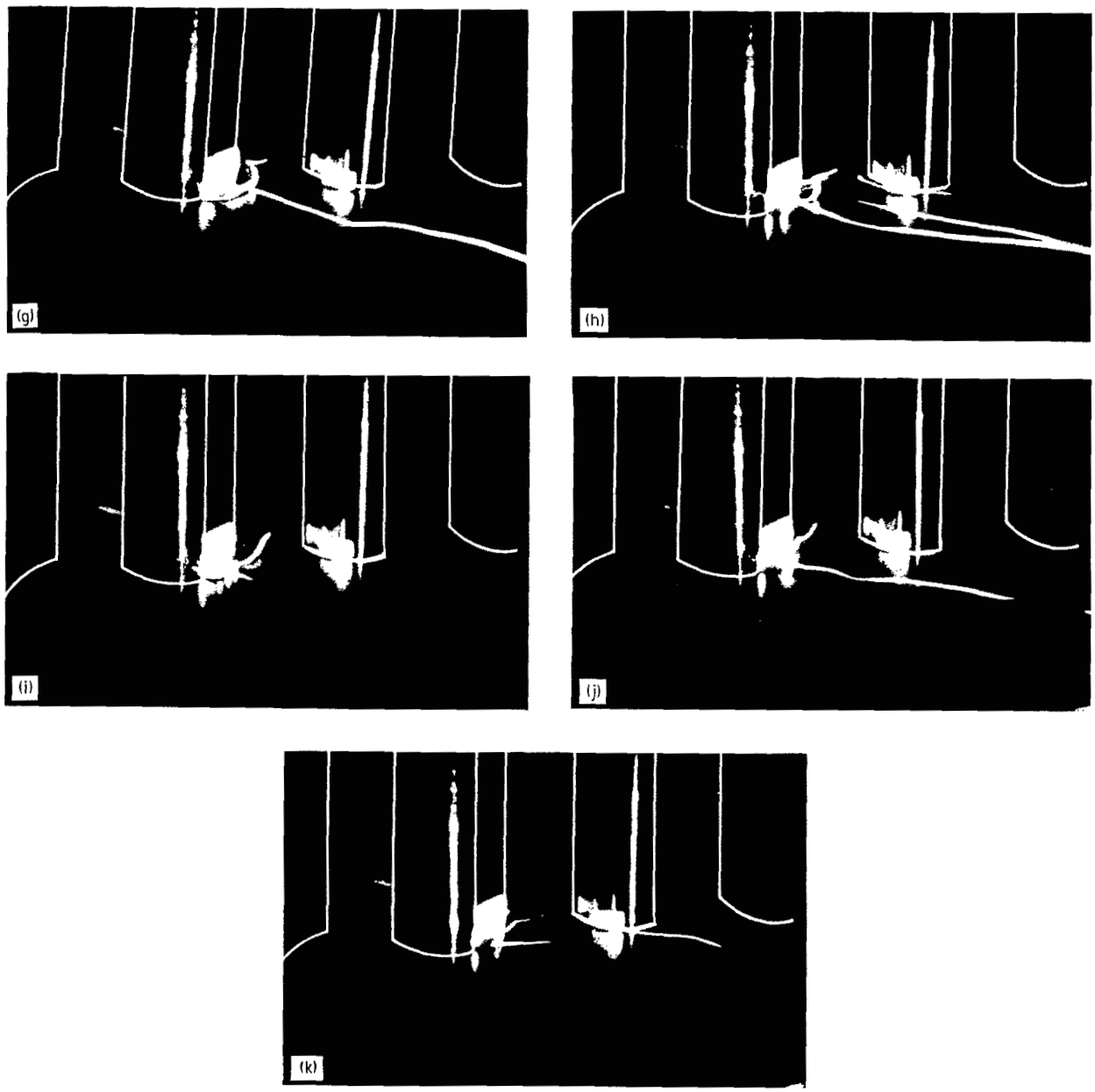

Figure 17. - Concluded.

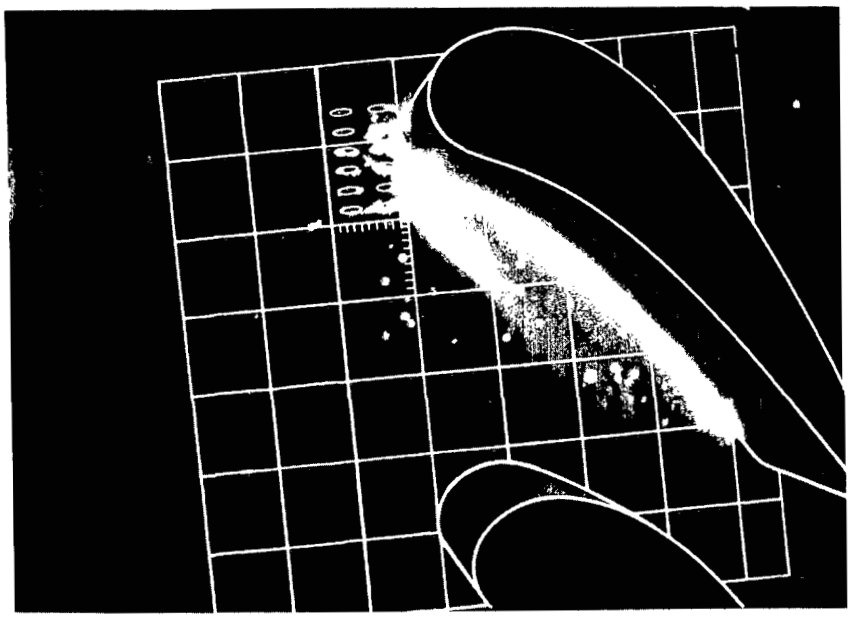

(a) Jet 1 off.

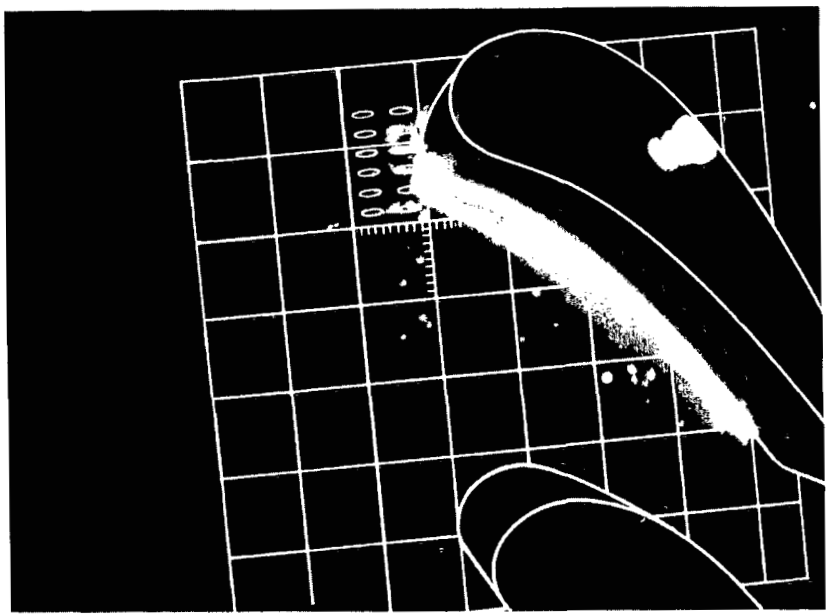

(b) Jet 1 on.

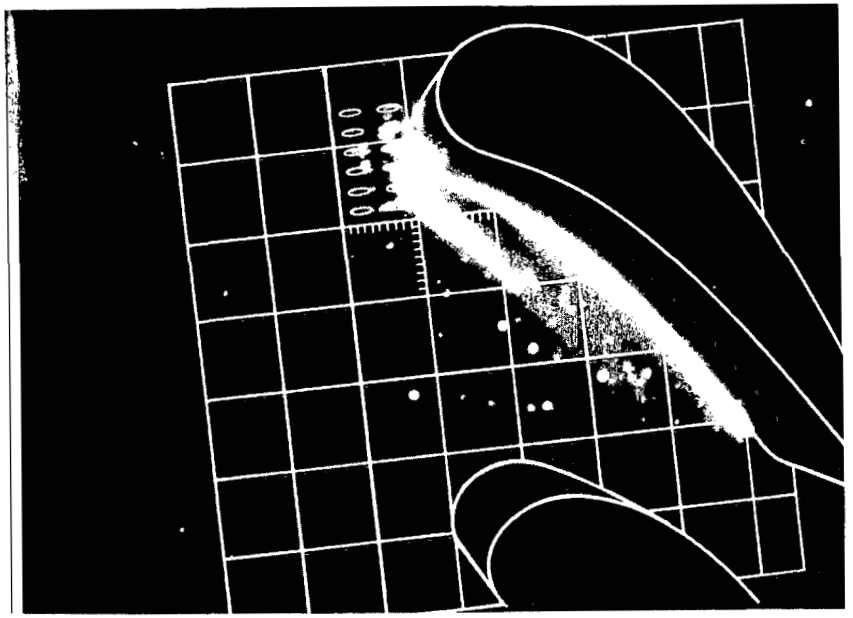

(c) Jet 2 off.

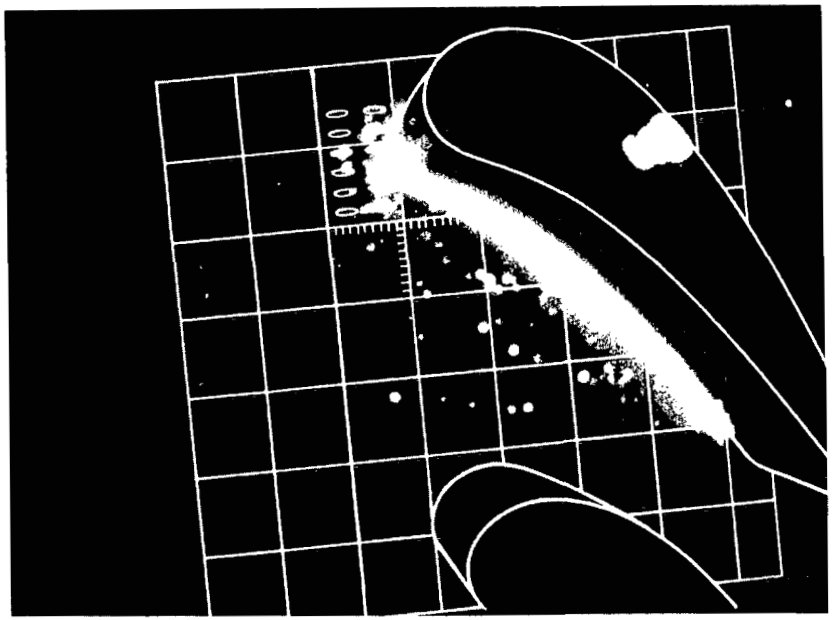

(d) Jet 2 on.

Figure 18. - Smoke in vortex, with control jets on and off.

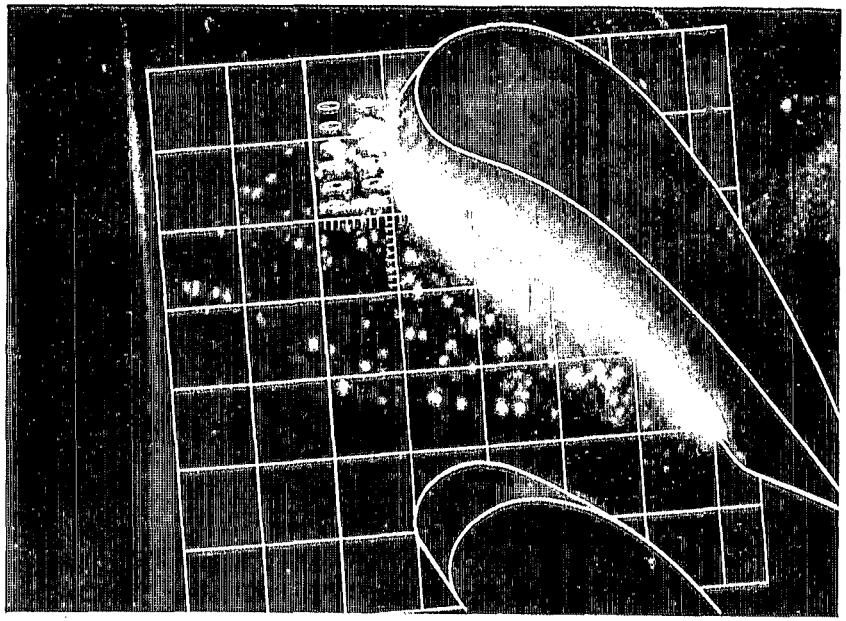

(e) Jet 3 off.

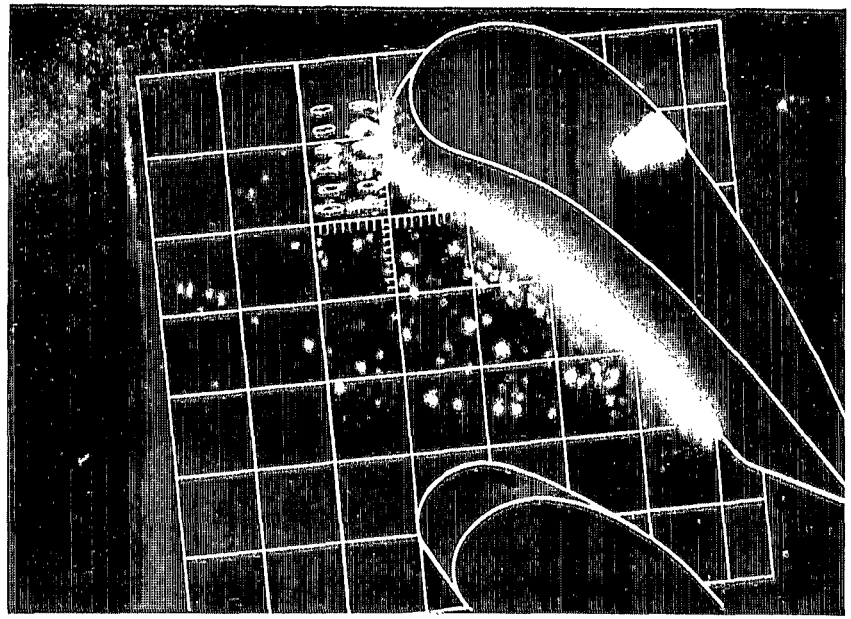

(f) Jet 3 on.

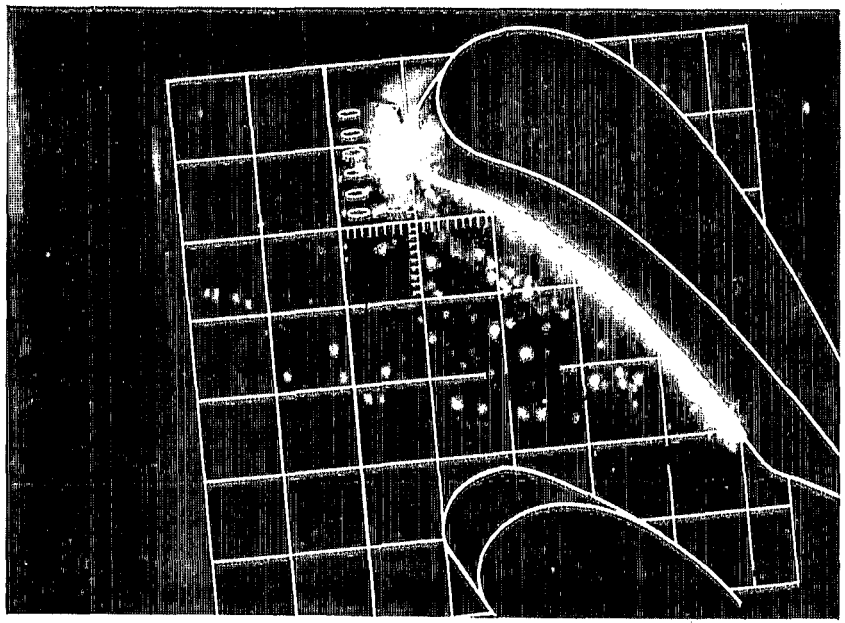

(g) Jet 4 off.

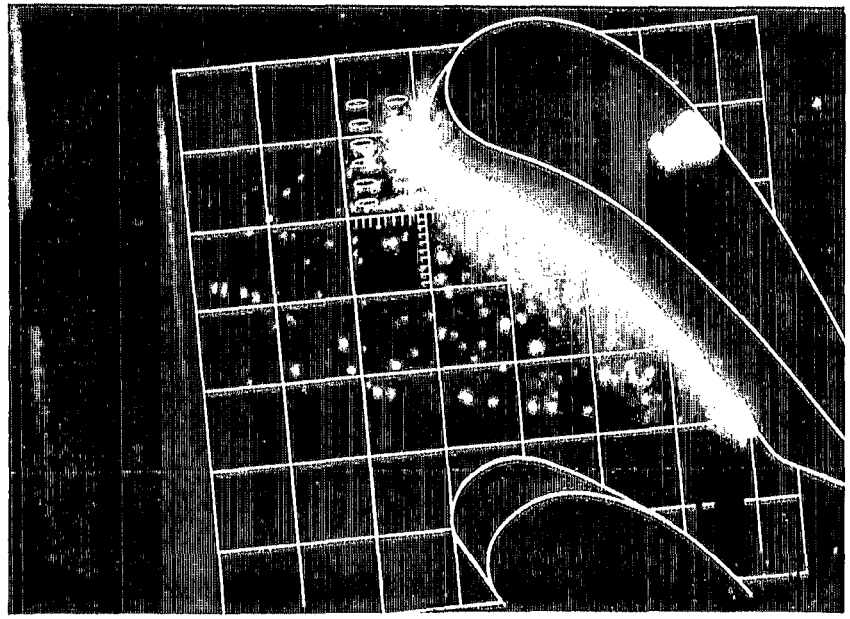

(h) Jet 4 on.

Figure 18. - Continued.

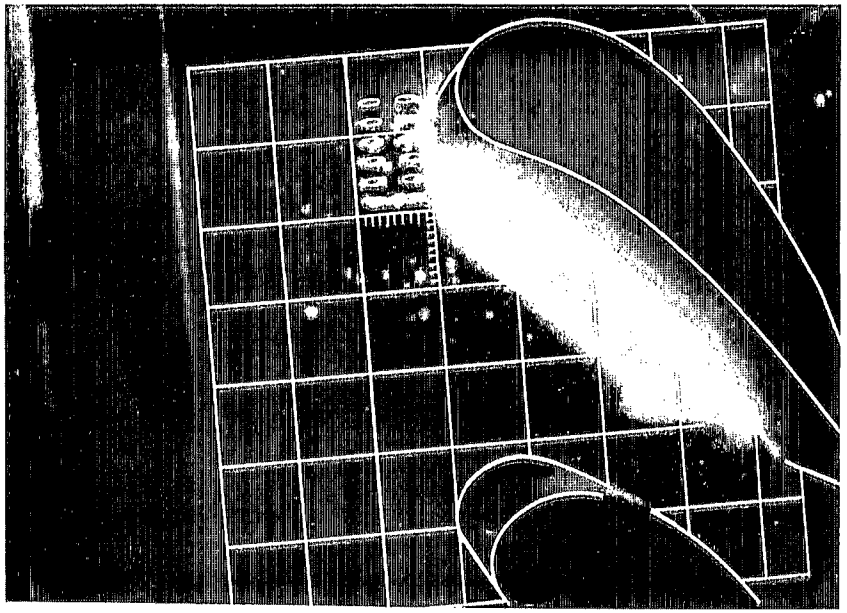

(i) Jet 8 off.

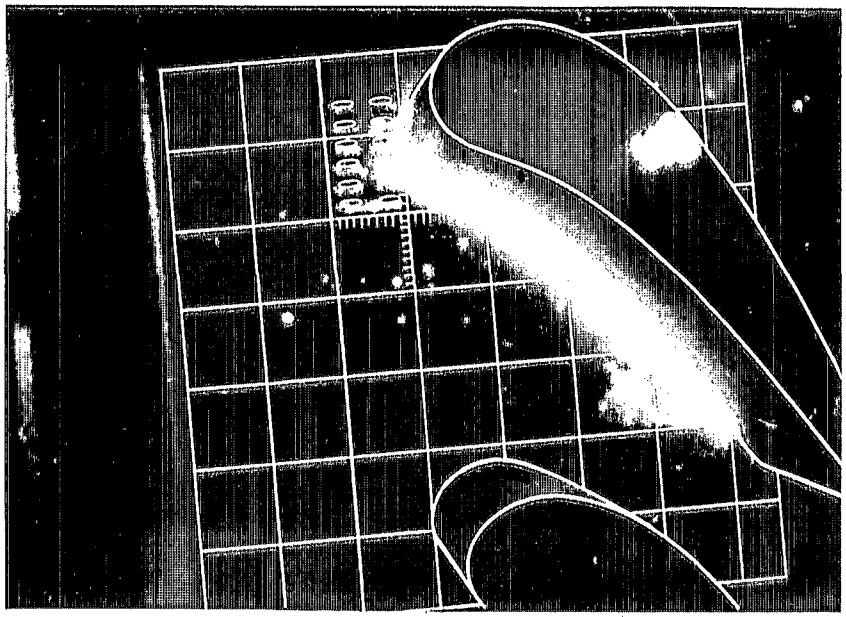

(j) Jet 8 on.

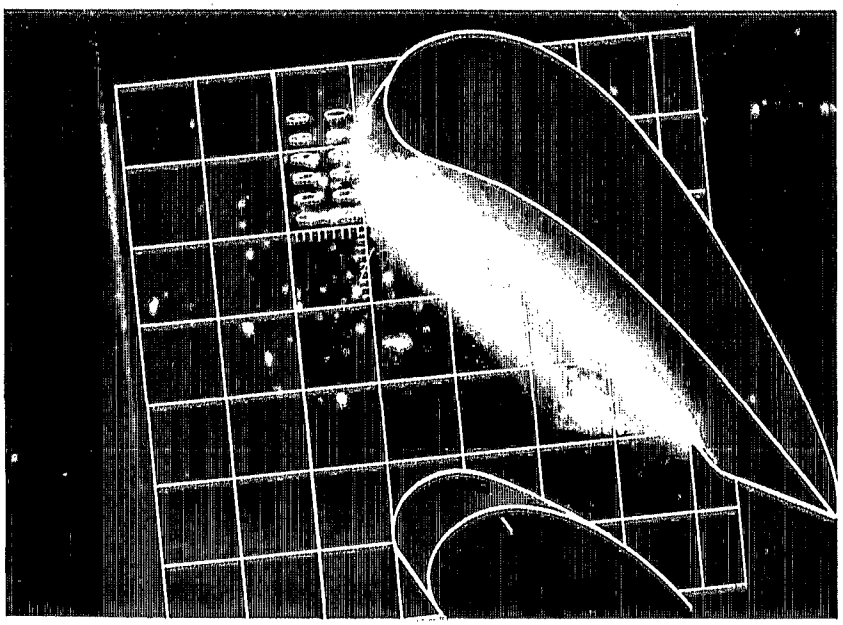

(k) Jet 9 off.

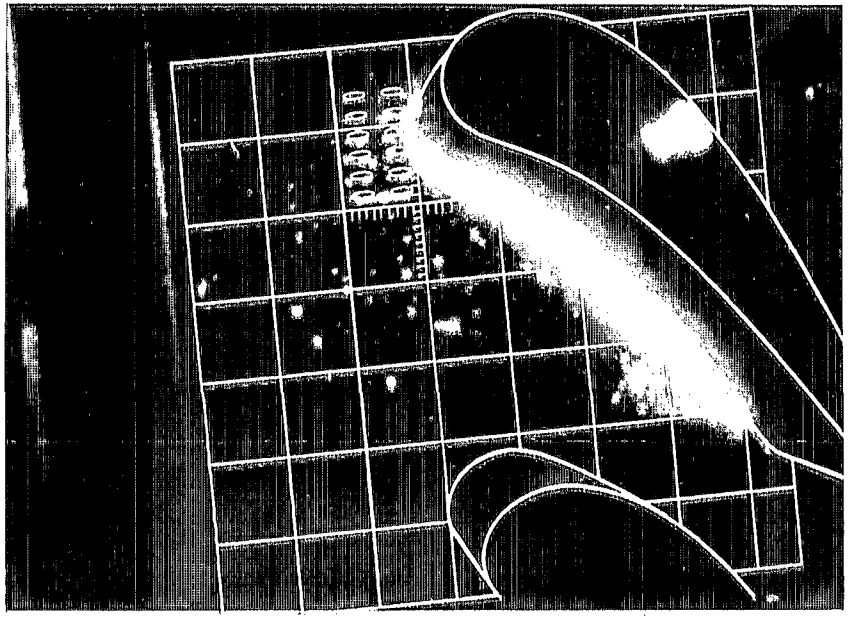

(l) Jet 9 on.

Figure 18. - Continued.

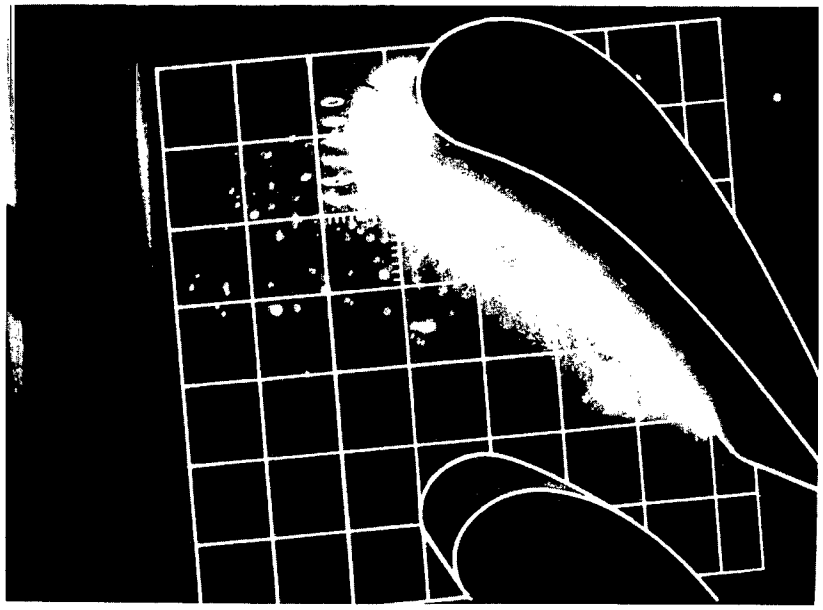

(m) Jet 10 off.

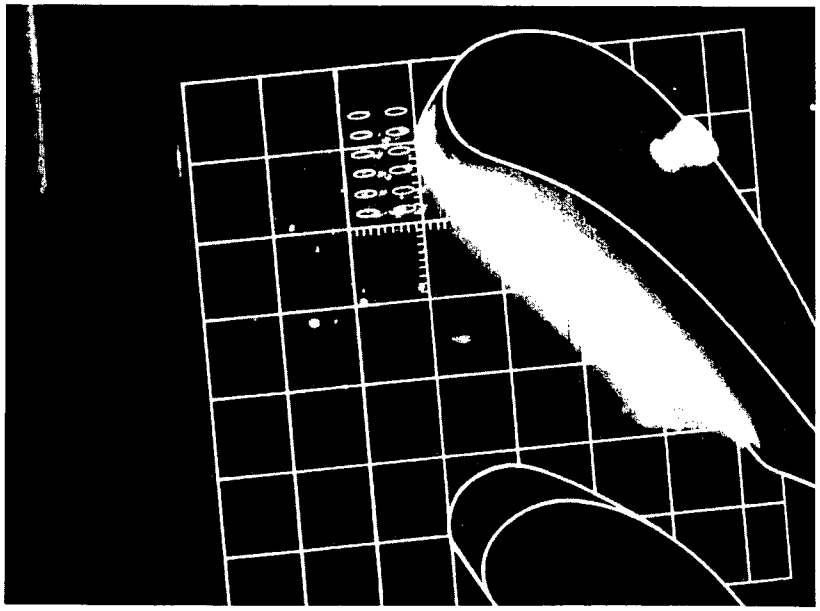

(n) Jet 10 on.

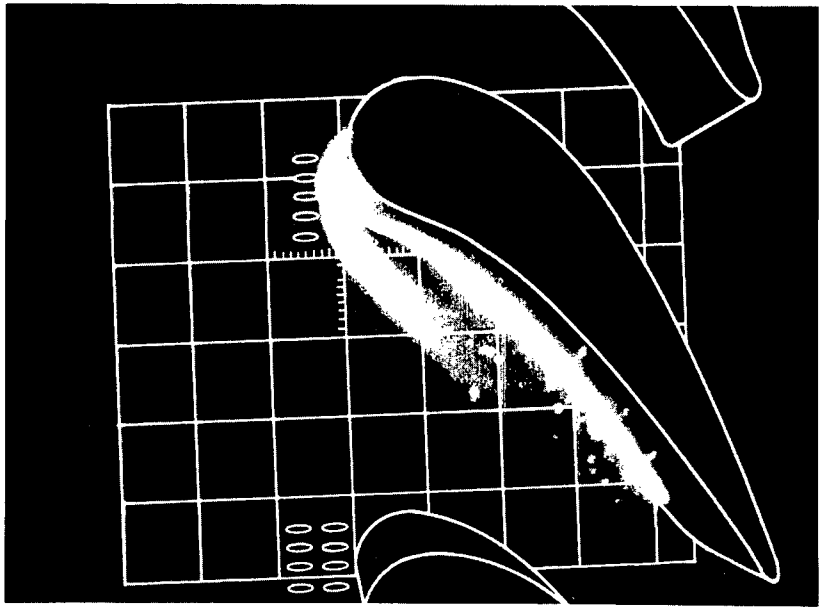

(o) Jet 13 off.

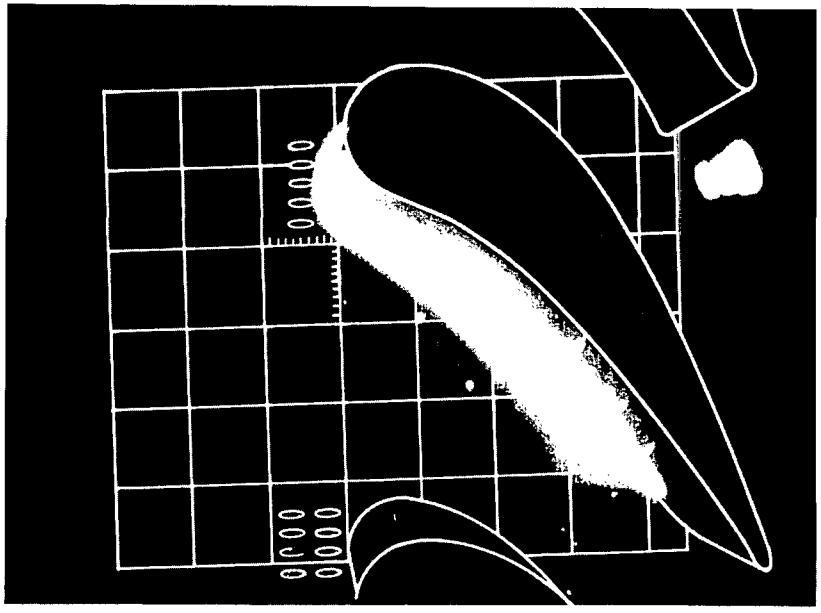

(p) Jet 13 on.

Figure 18. - Continued.

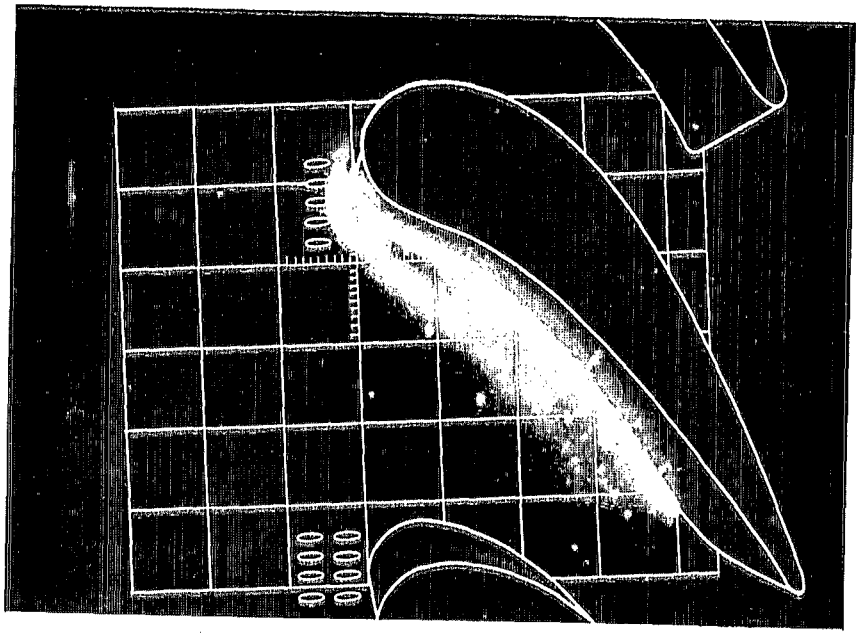

(q) Jet 14 off

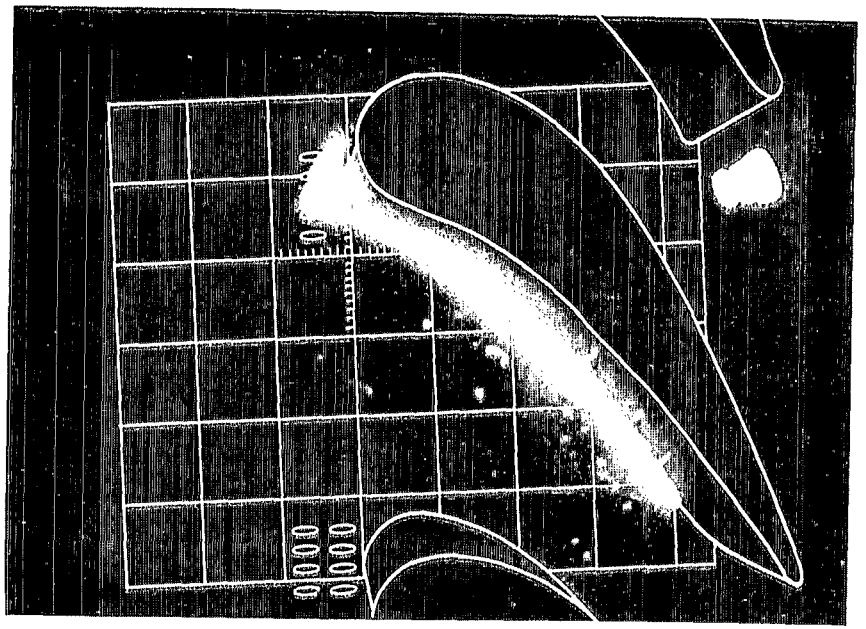

(r) Jet 14 on.

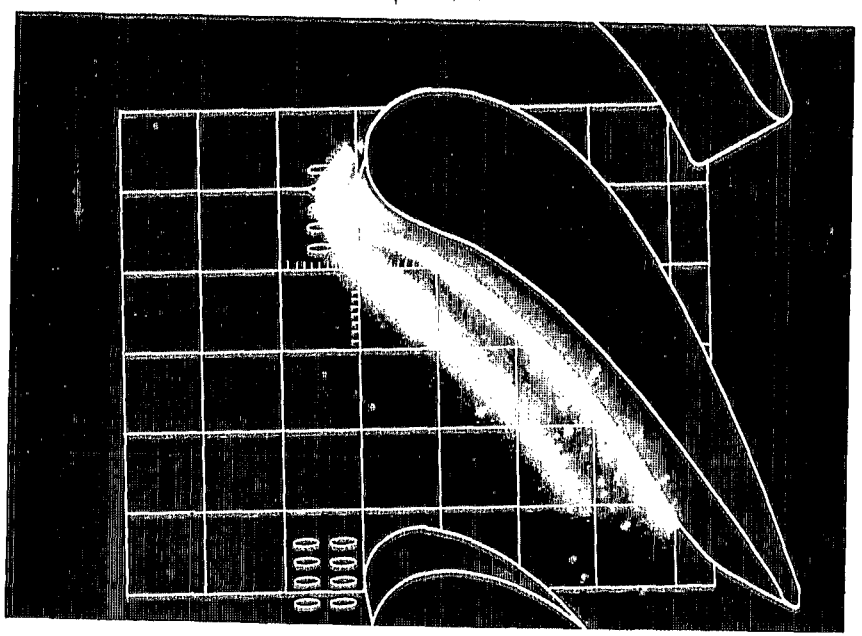

(s) Jet 15 off

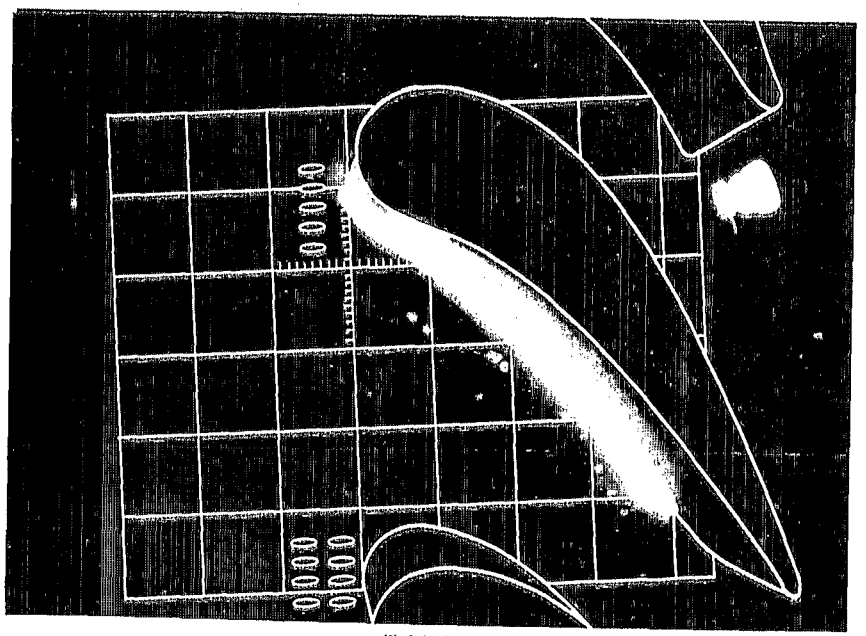

(t) Jet 15 on.

Figure 18. - Concluded.

Lewis motion-picture film supplement C–298 is available on loan. Requests will be filled in the order received.

The film (16 mm, 14 min, color, sound) is a flow visualization study of the horseshoe vortex in a turbine stator cascade. Through the use of oil drops on the end wall, smoke, and helium-filled soap bubbles, it is shown that the injection of film cooling air through the end wall does affect the horseshoe vortex. By guiding the analyst in constructing a mathematical model of turbine secondary flows, this study will result in more efficient use of end-wall cooling air, with subsequent improvement in engine performance.

Requests for film supplement C–298 should to be addressed to

NASA Lewis Research Center
Attn: Chief, Management Services Division (5–5)
21000 Brookpark Road
Cleveland, OH 44135

cut

Date _____

Please send, on loan, copy of film supplement C–298 to TP–1884

Name of Organization

Street Number

City and State Zip Code

Attention: Mr. _____

Title _____

1. Report No.	2. Government Accession No.	3. Recipient's Catalog No.
NASA TP-1884		

4. Title and Subtitle
FLOW VISUALIZATION STUDY OF THE HORSESHOE VORTEX IN A TURBINE STATOR CASCADE

5. Report Date
June 1982

6. Performing Organization Code
505-32-2B

7. Author(s)
Raymond E. Gaugler and Louis M. Russell

8. Performing Organization Report No.
E-915

9. Performing Organization Name and Address
National Aeronautics and Space Administration
Lewis Research Center
Cleveland, Ohio 44135

10. Work Unit No.

11. Contract or Grant No.

12. Sponsoring Agency Name and Address
National Aeronautics and Space Administration
Washington, D.C. 20546

13. Type of Report and Period Covered
Technical Paper

14. Sponsoring Agency Code

15. Supplementary Notes
Film supplement C-298 showing the flow visualization results is available, on request, from the NASA Lewis Research Center.

16. Abstract

Flow visualization techniques were used to show the behavior of the horseshoe vortex in a large-scale turbine stator cascade. Oil drops on the end-wall surface flowed in response to local shear stresses, indicating the limiting flow streamlines at the surface. Smoke injected into the flow and photographed showed time-averaged flow behavior. Neutrally bouyant helium-filled soap bubbles followed the flow and showed up on photographs as streaks, indicating the paths followed by individual fluid particles. Preliminary attempts to control the vortex were made by injecting air through control jets drilled in the end wall near the vane leading edge. Seventeen different hole locations were tested, one at a time, and the effect of the control jets on the path followed by smoke in the boundary layer was recorded photographically. A motion picture supplement is available.

17. Key Words (Suggested by Author(s))	18. Distribution Statement
Horseshoe vortex End walls Boundary layer	Unclassified - unlimited STAR Category 34

19. Security Classif. (of this report)	20. Security Classif. (of this page)	21. No. of Pages	22. Price*
Unclassified	Unclassified	33	A03

* For sale by the National Technical Information Service, Springfield, Virginia 22161

NASA-Langley, 1982